ACS OMEGA

Open Access

http://pubs.acs.org/journal/acsodf

Article

Inhibition of the SARS-CoV-2 Non-structural Protein 5 (NSP5) Protease by Nitrosocarbonyl-Bases Small Molecules

Marco Leusciatti, Beatrice Macchi, Francesca Marino-Merlo,* Valeria Stefanizzi, Antonio Mastino, Giulia Morra,* and Paolo Quadrelli*

Cite This: *ACS Omega* 2024, 9, 41599−41615

Read Online

ACCESS | Metrics & More | Article Recommendations | Supporting Information

ABSTRACT: In the present work, we have designed and synthesized potential NSP5 protease allosteric inhibitors exploiting both docking and molecular dynamic data on SARS-CoV-2. The chemical protocols were developed on the basis of 1,3-dipolar cycloaddition reactions as well as the chemistry of nitrosocarbonyl intermediates. Computational studies were first conducted for determining the best candidate for SARS-CoV-2 NSP5 protease inhibition. Selected compounds were submitted to biological tests, showing low cytotoxicity and moderate activity.

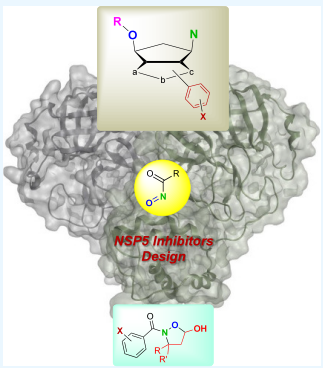

INTRODUCTION

The devastating coronavirus disease 2019 (COVID-19) pandemic caused by SARS-CoV-2 is challenging us both in public health policies and in pharmacological tools. Since the first detection in Wuhan, China in December 2019, of the novel coronavirus, successively named SARS-CoV-2, the virus has rapidly started to evolve. The virus diverged into new strains due to mutations; these strains initially resembled the ancestral strain greatly but gradually evolved further to create more diverse mutants. Numerous variations of SARS-CoV-2 were documented subsequent to the first virus outbreak. The World Health Organization (WHO) has designated certain variants as variants of concern (VOC) due to their influence on world health, through evaluation of an increase in transmissibility or an increase or modification in clinical presentation.[1] Despite vaccination success, a worldwide uneven distribution of doses, vaccine hesitancy in the population, emergence of virus variants, and noticing of limited duration of protective immunity made eradication an unlikely outcome and highlighted the need for efficacious pharmacological treatments.[2] In a recent paper,[3] we have discussed about the critical aspect of the lack of effective antiviral therapeutics to treat COVID-19 patients and the repurpose of antivirals already approved exhibiting inhibitory activity against either proteases (Lopinavir, Ritonavir) or RNA-dependent RNA-polymerases (RdRp) of other viruses (Remdesivir, Favipiravir).[4] Our studies focused attention on the role of isoxazoline-carbocyclic monophosphate nucleotides, designed and synthesized through the nitrosocarbonyl chemistry with the help of the stable anthracenenitrile oxide, in docking and molecular dynamic investigations that were first conducted for determining the best candidate for polymerase SARS-CoV-2 inhibition. The setup phosphorylation protocol afforded the nucleotides available for the biological tests. Preliminary inhibition and cytotoxicity assays were then performed and the results showed a moderate activity of the nucleotides accompanied by citotoxicity.[3]

These recent determinations also oriented the development of antiviral drugs targeting viral proteases. The SARS-CoV-2 nonstructural protein 5 (NSP5) viral protease, also known as the main protease (M^{pro}) or 3-chymotrypsin-like protease (3CLpro) is highly conserved, showing a 3-chymotrypsin-like fold (Figure 1).[5]

Coronaviruses are known to exhibit a high degree of conservation, with the *N*-terminal domains (1 and 2) forming a 3CLpro fold made up of β-barrels. The catalytic site of SARS-CoV-2 and SARS-CoV-1 NSP5 proteases contains two highly conserved residues, namely His41-Cys145.[1,6]

Hence, the mature form of NSP5 protease is dimeric, with individual monomers having reduced enzymatic activity. The dimeric form of NSP5 functions as a functional unit with maximum hydrolytic activity. One of the essential prerequisites for the formation of dimeric NSP5 protease is a strong binding

Received: June 12, 2024
Revised: August 9, 2024
Accepted: August 20, 2024
Published: September 25, 2024

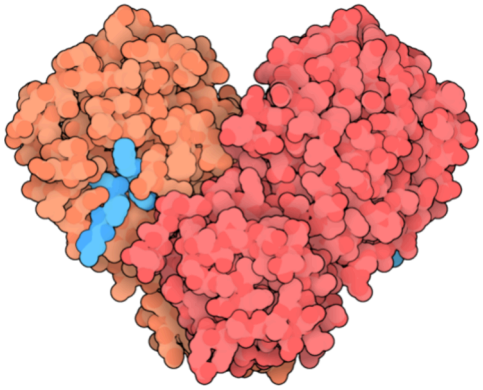

Figure 1. SARS-CoV-2 NSP5 protease as a dimer from protomers A and B.

between the *N*-finger and *C*-terminus, particularly the salt bridges of Arg4 and Arg298. The NSP5 protease catalytic site is situated where domains I and II converge.[7]

The identification of anti-SARS-CoV-2 medicines finds NSP5 to be a highly interesting target due to its key function in the viral life cycle and the absence of comparable proteins in human cells. The therapeutic effectiveness of HIV and HCV protease inhibitors indicates that targeting proteases is a viable avenue for the identification of antiviral drugs. Several strategies can be used to inhibit these enzymes; in fact, the development of reversible, covalently reversible, and irreversible binders has been utilized in a variety of therapeutic contexts, including the development of antivirals.[8]

Allosteric inhibitors have also been considered as a modulation strategy for SARS-CoV-2 and other human CoVs by high throughput screening approaches[9] and rational design.[10] Some allosteric sites were recently mapped on the NSP5 protein for CoVs and a few complexes with cocrystallized ligands, specifically binding one of the sites emerged (Figure 2).[11] These inhibitors generally show a lower

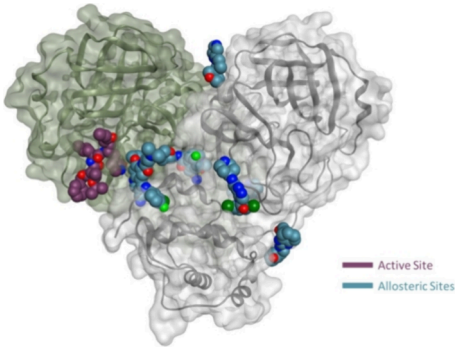

Figure 2. Representation of the NSP5 protease enzyme in the dimeric form, along with cocrystallized ligands in either active site and in experimentally proven allosteric sites. Reproduced with permission from ref 14. Copyright © 2022; originally published by and used with permission from Dove Medical Press Ltd.

resistance barrier with respect to molecules directly targeting the active site and are characterized by drug-like heterocyclic scaffold; thus, the identification of such agents may offer the advantage of handling molecules with higher optimization potential.[12−14]

Reasonable targeting of alternative sites might therefore provide innovative ways to disrupt protein−protein (PP) interactions, which are widely acknowledged as difficult targets as well as novel chemotypes for possible inhibitors.

The search for new compounds for the treatment of viral diseases and selective antiviral chemotherapy is being actively pursued in the Pavia's group, and various scaffolds were proposed toward this goal. Since 1996, we have been investigating original synthetic methodologies in organic chemistry to achieve chemical compounds behaving as antiviral compounds.[15] Our approach promoted the pericyclic reactions and the chemistry of nitrosocarbonyls, a family of fleeting intermediates suitable for the stereochemical ordinate introduction on carbocyclic scaffolds of functional groups suitable for several and variable functionalizations.[16]

We explored the chemical space built in the past 20 years and belonging to two main categories: (i) compounds obtained through the hetero Diels−Alder cycloaddition[17] of nitrosocarbonyl **1** to cyclopentadiene and synthetic elaboration of the primary cycloadducts[18] (Scheme 1, top) and (ii) ene addition[19] of nitrosocabonyl intermediates to allylic alcohols or alternative method though hydroxamic acids with unsaturated aldehydes[20] (Scheme 1, bottom).

Scheme 1. Chemical Design of Novel SARS-CoV-2 Protease Inhibitors

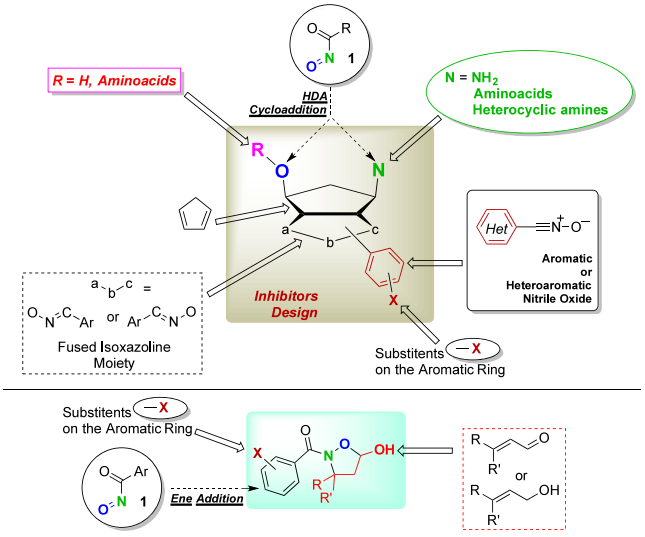

The exact structures that will be here presented (*vide infra*) were submitted to modeling studies aiming to direct/orientate both the selection and the synthetic strategies and suggest eventual/consequent structural design changes within the chosen chemical compounds. Second, biological evaluations through antiviral and cytotoxicity tests will give immediate and preliminary responses on the activity of the prepared compounds, providing helpful feedback for concentrating the efforts of modeling and synthesis toward the most promising molecules, *post* this preliminary evaluation.

It clearly appears that the pivotal combination of these three pillars [*modeling⇔chemistry⇔-in vitro tests*] that are highly connected and integrated and the results of any advancement in one area generate effects in the others in a continuous way, thus fulfilling the application of pericyclic reactions in this new Proof of Concept (POC) devoted to the inhibition of SARS-CoV-2 proteases.

A viral target-oriented production of small molecules able to display some biological activity compatible with an antiviral

https://doi.org/10.1021/acsomega.4c05480
ACS Omega 2024, 9, 41599−41615

activity to be ascertained and suitable for further development under structural modification suggested by computational analysis and extensive biological tests is here presented and discussed. We expect that the selected decorated scaffolds could find interesting applications in the present investigation on drug design/development due to the intrinsic characteristics of their structural and electronic properties from a medicinal chemistry point of view (i.e., minor degrees of freedom of movement are allowed for a ring system compared to linear system, elevated number of intrinsic pharmacophoric features, regio- and stereo-ordered introduction of substituents).

RESULTS

Computational Analysis. *Clustering and Allosteric Site Selection.* The strategy we set out for inhibiting NSP5 relies on the rationale that the protein works as a dimer, and destabilizing the dimerization interface might disrupt the catalytic function, as shown by point mutation experiments.[6] Therefore, aiming at finding suitable targeting sites, we took advantage of Molecular Dynamics (MD) simulations to explore possible pockets in the vicinity of the dimerization surface that were enhanced during the protein functional motions.[21] To this end, we combined the clustering analysis of a 442 ns MD simulation of the dimer with site mapping to locate the candidate binding pockets. Figure 3 shows the workflow that was used to obtain the protein structures for screening and computational analysis. The 442 ns dynamics of the NSP5 dimer available on the SCoV2-MD.org repository was analyzed and subjected to Cα clustering analysis performed with GROMACS (see Methods), to identify the dynamic-derived structures of SARS-CoV-2 NSP5 considered for pocket mapping (see Methods for details).[22]

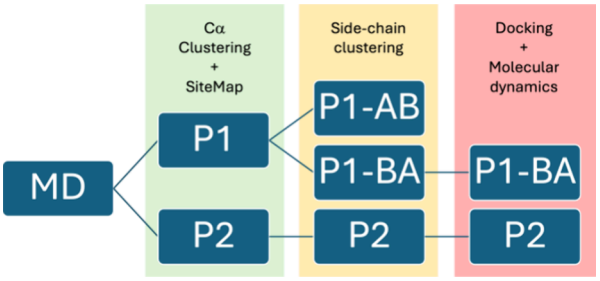

Figure 3. Workflow used to obtain the protein structures for allosteric sits selection for the docking screening and subsequent molecular dynamics of complexes.

Guided by our hypothesis for the protease activity inhibition through destabilization of the dimer interface, among the identified pockets, we focused on the ones closer to the PP interface, having the best druggability scores according to pocket size, hydrophobicity, and enclosure (see Methods) and comprising conserved residues. We finally selected two putative pockets, which we called "Proximal Site" represented by *Pocket 1* (*P1*) and the "Dimerization Site" namely *Pocket 2* (*P2*) as shown in Figure 4.

After locating the relevant sites *P1* and *P2*, we then proceeded with a more focused side-chain clustering analysis, to characterize the pocket shape and interaction points (see Figure 3 and Methods). The representative structure of the most populated cluster for each pocket was then selected as the target (Figure 4).

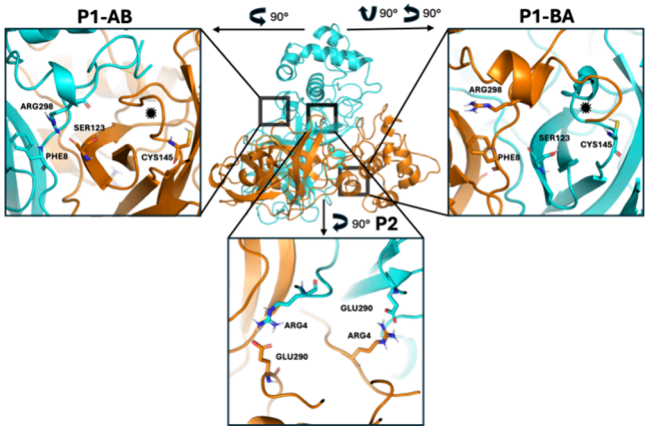

Figure 4. Illustration of the allosteric pocket location in the NSP5 dimer (top center): chain A in cyan, chain B in orange. Representation of *P1* (P1_AB top left and P1_BA right) and *P2* (bottom) in the NSP5 dynamic-derived structures. In *P1* residues Phe8, Ser123, Cys145, and Arg298, are indicated, with C-loop highlighted by the black asterisk. In *P2*, the salt-bridge-forming residues Arg4 and Glu290 are indicated.

Proximal Site P1 is a superficial pocket located near the PP interface close to the catalytic site (see Figure 4, Cys145). Interestingly, *P1* was found in a different conformation at each chain interface (chain AB; chain BA) despite starting crystal symmetry. The Dscores (see Methods) were similar between the two: *P1*-AB Ds = 1.059; *P1*-BA Ds = 1.057. In contrast, the volumes pointed to a more disclosed cavity at the BA interface with respect to AB, 624 and 431 Å^3, respectively. This is due to the lifting of Arg298 of chain B losing the H-bond with Ser123 of chain A. Arg298 proved essential for both dimerization and enzymatic activity by point mutation experiments: namely, replacement of Arg298 by Ala resulted in an inactive and monomeric form of the enzyme.[6]

Notably, the flip of Arg298 in the analyzed MD simulations of BA allow the C terminal tail reaching the catalytic site, inducing the switch of the C-loop (residues 138−143) collapsing the oxyanion hole stabilizing the catalytic intermediate.[23]

Dimerization Site P2 (see Figure 4) presented a slightly lower Dscore, Ds = 1.035, but bigger volume (788 Å^3), more enclosure e_x = 0.44, and higher hydrophilic character of p = 1.25 with respect to p = 0.88 of *P1*. It is more deeply inserted in the dimerization interface and is symmetric. It targets several high-energy hot spots within the dimerization interface, such as residues Ser1, Arg4, Lys5, and Glu290, which create salt bridges between the two monomers, necessary for NSP5 dimerization.[11]

Docking and Molecular Dynamics. The two previously identified pockets of SARS-CoV-2 NSP5, *P1* and *P2*, were considered in a virtual screening approach and enriched by MD analysis of the complexes, which was carried out in parallel for both pockets. 586 molecules from the available set of synthesizable compounds were first docked one by one. Then, complexes with potential binders showing good ligand efficiencies (see Methods) as well as specific interactions with pocket residues hypothesized as essential were selected for further analysis.

The structures of the selected compounds binding to pocket *P1* are shown in Figure 5 and are numbered according to the respective entry in the compiled database.[24,25]

https://doi.org/10.1021/acsomega.4c05480
ACS Omega 2024, 9, 41599−41615

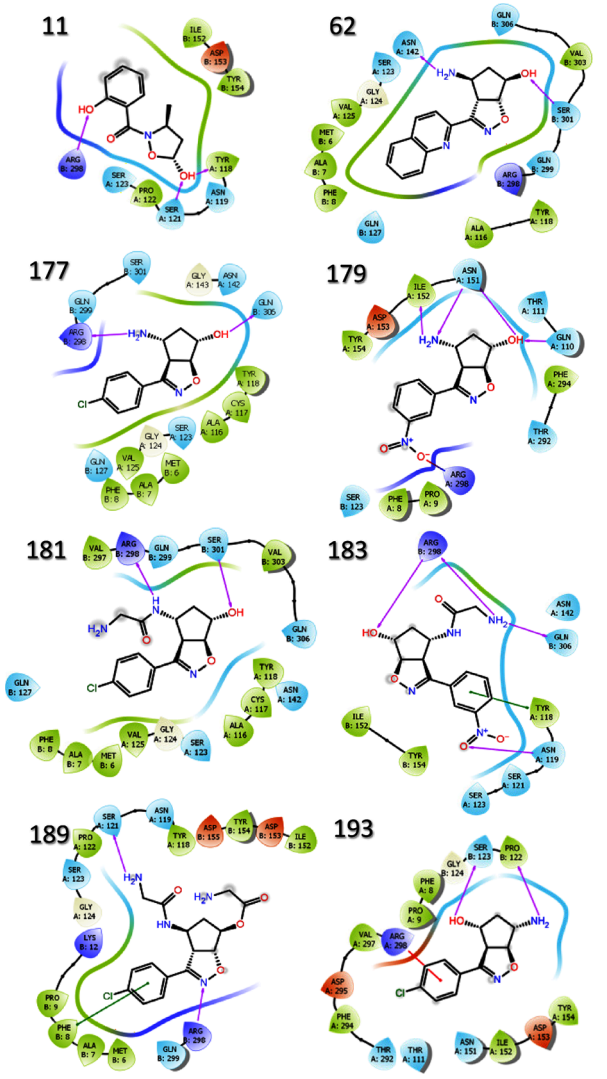

Figure 5. LIDs in 2D workspace of selected compounds: **11**, **62**, **177**, **179**, **181**, **183**, **189**, and **193** docked in *P1*-BA. Magenta arrows: H-bond; red lines: π-cation; green lines: π-stacking; red to blue gradient strip: salt bridge.

For *P1*, docking poses were selected by their scores, ligand efficiencies and presence of an interaction with Arg298 (see Table S1 in the Supporting Information), due to the reported role in dimerization process. Figure 5 shows the Ligand Interaction Diagrams (LIDs). Molecules can establish different kinds of interactions with Arg298, such as stacking in the case of quinoline derivative **62** and π-cation for the p-chlorine substituted aminol **193** or a salt bridge with the *m*-nitro group of aminol **179**, hydrogen bonds with heteroatoms in **177**, and in the case of mono- or bisubstituted aminols, **181**, **183**, and **189** H-bonds too.

The second set of putative ligands was obtained by screening the compound data set on the dimerization pocket *P2*. After performing virtual screening on *P2*, compounds were ranked by docking score and ligand efficiency (see Table S2 in the Supporting Information). Moreover, this time interaction with protein residues Arg4, Lys5, Ser10, Gly11, Glu14, Glu288, and Glu290 was considered as a selection criterion, given their reported role in dimerization and our working hypothesis that perturbing the high energy hotspots present at the interface at *P2* might lead the transition of the protein from the dimeric to the monomeric state, losing its activity.[13,14,21−24] Figure 6 shows the LIDs of the designed compound selected from the

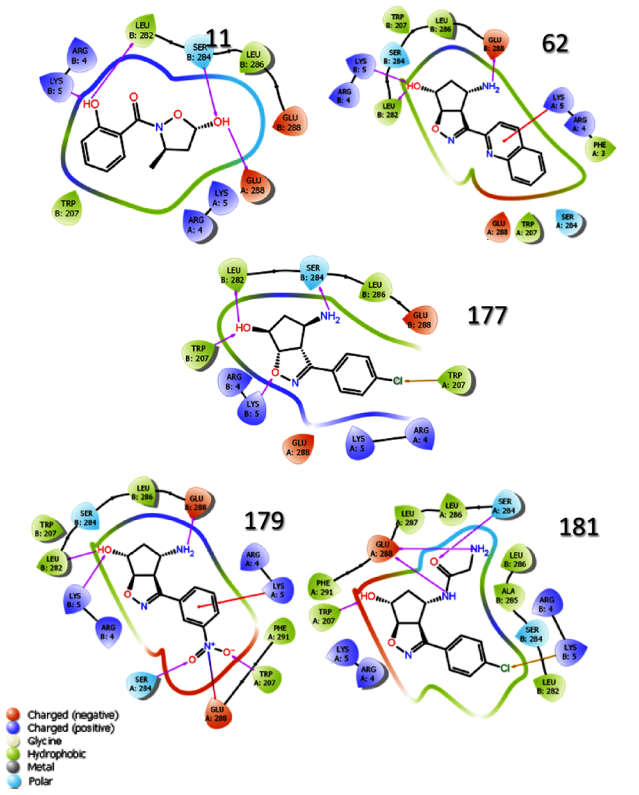

Figure 6. LIDs in 2D workspace of selected compounds **11**, **62**, **177**, **179**, and **181** docked in *P2*. Magenta arrows: H-bond; red lines: π-cation; green lines: π-stacking; red to blue strip: salt bridge; yellow: halogen bond.

docking screening. The structures of the selected compounds docked into *P2* are numbered according to the respective entries in the compiled database.

The selected compounds for *P2* mainly belong to the aminol family, and all displayed excellent ligand efficiencies. The interactions with amino acids responsible for dimer stabilization vary remarkably. Hydrogen bonding interactions of 5-hydroxy-isoxazolidine **11** constitute a link between Ser284 and Glu288. The quinoline-substituted aminol **62** shows two different interactions: hydrogen bonding and an π-cation with each Lys5 of the monomers and Glu288. A network of H-bonds with the heteroatoms of the aminolic scaffolds as well as halogen bonds are observed in the case of *p*-chlorine substituted aminol **177** while a π-cation and a salt bridge are established by the *m*-nitro substituted compound **179**. Finally, hydrogen bonding with the amino acid residues is shown in the case of isoxazoline **181**.

To further investigate the potential of selected compounds as allosteric inhibitors, the best docking poses of each selected ligand, either in *P1*, in *P2*, or in both, were subjected to 50 ns of MD, in which the ligand stability and some protein structural and dynamic parameters were evaluated. Specifically, to make a prediction on allosteric effects on the dimerization state of the protein or on the stability of the catalytic site upon ligand binding, three key distances were evaluated, comparing apo protein (i.e., protein without the prosthetic group) and

https://doi.org/10.1021/acsomega.4c05480
ACS Omega 2024, 9, 41599−41615

molecule complexes (see Figure 7), namely, Arg298-Ser123, Arg4-Glu290, and Cys145-His41.

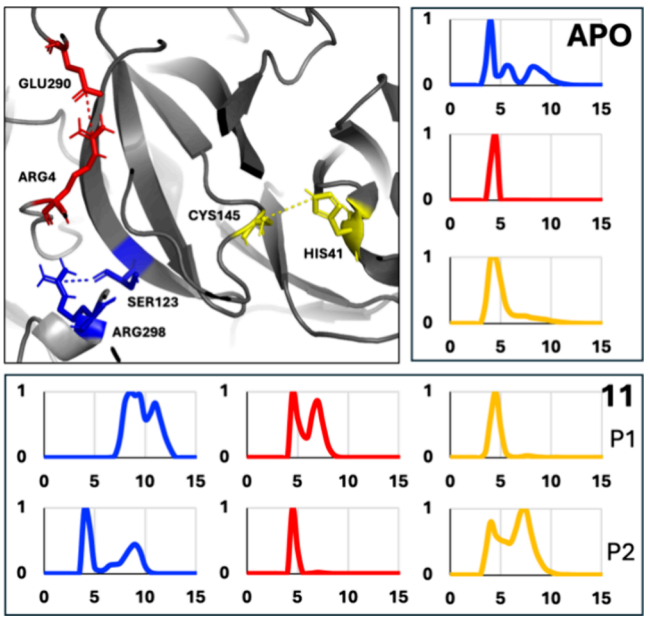

Figure 7. Evaluated amino acid residue pair distances (Å). Highlighted residues Arg4 and Arg298, in blue, are part of chain B while His41, Cys145, in yellow, and Arg4 and Glu290, in red, belong to chain A (top left). Distribution of key distances between residues Arg298-Ser123 (blue), Arg4-Glu290 (red), and Cys145-His41 (yellow) of the apo NSP5 (top right) and of the compound **11** (bottom), as emerging from MD trajectories.

The distance between residues Arg298-Ser123 represents local effects at the dimer interface (blue), the Arg4-Glu290 distance accounts for the dimer stability (red), and the Cys145-His41 distance reports on the productive state of the catalytic dyad (yellow) of the apo NSP5. The red and blue distances are proximal to *P1*, whereas *P2* is located at a distance of about 26 Å from the catalytic site.

The isoxazolidine **11**, while stable in pocket *P2* (see Figure S1 in the Supporting Information) upon 50 ns MD, in pocket *P1* reorients from the initial binding pose and buries itself under Arg298. A snapshot at the end of the simulation reveals that **11** reproduces the binding pose of two known cocrystallized fragments: the sulfamide **x1086** (PDB: 5RGQ) and the pyrazole **x1187** (PDB: 5RFA) derivatives (Figure S1 in the Supporting Information). The pyrazole is reported to disrupt the dimer, leading to a decrease of turnover rate of NSP5.[25]

The distribution of the key distances along the MD simulation is reported in Figure 7 for compound **11** and for the apo system for comparison. When bound to *P1*, compound **11** destabilizes the dimer (red line) by increasing the Arg4-Glu290 distance from 4.5 to 7 Å. The Cys145-His41 distance (yellow line) is unperturbed. In contrast, when bound to pocket *P2*, it appears to destabilize the Cys145-His41 distance and leave mostly unchanged the others.

Concerning the isoxazoline-cyclopentane aminol derivatives (see structures in Figures 5 and 6), effects on the amino acid pair distances are also observed in MD simulations and the plots are gathered in Figure 8 for the subset of ligands that, showing some local perturbation signal in at least one of the pockets, were subsequently tested.

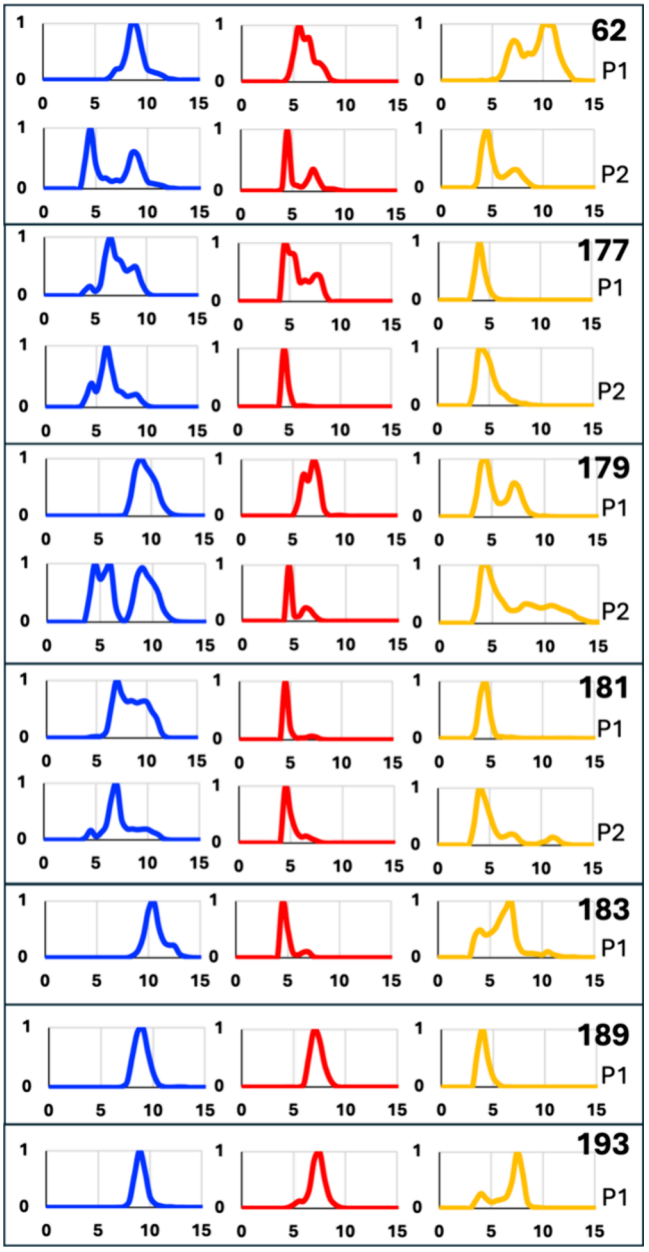

Figure 8. Molecular dynamics distribution of key distances (Å) between residues Arg298-Ser123 (blue), Arg4-Glu290 (red), and Cys145-His41 (yellow) of complexes formed by compounds **62**, **177**, **179**, **181**, **183**, **189**, and **193** (from top to bottom) when bound to the specified pockets.

Analyzing the results for *P1*, the quinoline aminol **62**, impacted dimerization (red line), broadening the distribution to higher values with respect to the apo system, and on the productivity of the catalytic dyad too, showing a peak at a greater Cys145−His41 distance of 11.7 Å. Along the simulation, **62** never left the pocket as shown by the low rmsd (see Figure S7 in the Supporting Information).

Conversely, for the aminol **177** the rmsd (see Figure S7 in the Supporting Information) was significantly higher, it displayed a more erratic behavior moving away from Arg298, which was reflected in minor allosteric effects. There was no appreciable perturbation of the catalytic dyad (yellow distribution) but it at least induced moderate destabilization of the dimerization with a small peak at 7.7 Å.

https://doi.org/10.1021/acsomega.4c05480
ACS Omega 2024, 9, 41599−41615

In pocket *P1*, compound **179** induces moderate allosteric effects on the catalytic site (yellow distance, average 5.3 Å), still perturbing Arg4-Glu290 interactions, leading to an average distance of 6.5 Å (red line). A similar perturbation at the red line is observed for compound **189**.

The glycine-substituted aminol **181** does not appear to be stable in *P1* behaving somehow like compound **177**, moving away from Arg298. It does not induce any effect on both dimerization and catalytic productivity as the distributions of distances stay centered on the apo system values.

When bound to pocket *P1*, compound **183**, despite occupying the pocket for the entire simulation, has no effects on dimer stability; nevertheless, it is somehow able to affect the catalytic dyad leading to an average distance of 5.9 Å. The aromatic ring remains buried in the pocket with the nitro group facing Arg298. The heteroatoms of the isoxazoline ring alternatively establish hydrogen bonds with the hydroxyl group of the side chain of Ser123. The glycine substituent keeps floating and interacting mainly with water molecules, so it does not contribute to binding.

The aminol **193** induces a mean distance of Arg4-Glu290 of 7 Å (red line) and pushes Cys145 apart from His41 at a 6.6 Å distance, placing it into the hypothesized active group. Despite lower interaction fractions, remarkably higher conformational changes appear in the pivotal C-loop region, bringing the catalytic Cys145 to face Asn142, differently from all the other complexes in both catalytic sites and apo. In addition, the turn Tyr118-Ser123 of chain A is shifted away from the PP interface.

When looking at *P2* complexes, compounds **11** and **179** show high values for the catalytic dyad distance Cys145-His41, which, in general, appears to be more perturbed by ligands in this pocket. In compound **11**, the Arg4-Glu290 distance is not affected at all, while the Cys145-His41 distance peaks at 7.5 Å. On the other hand, compound **179** presents a small peak at 6.1 Å in the distribution of the red distance, due to H-bond interactions of the heteroatoms of the isooxazoline with Arg4, and has a broader catalytic dyad distance distribution. It is also worth mentioning that **179** presents the highest separation between the residues involved in catalytic activity, reaching 15.21 Å, while **11** maxed out at 9.88 Å. Both appear to be stable in the pocket, as confirmed by the low rmsd (see Figure S7 in the Supporting Information).

Ligand **177**, despite destabilizing the dimer to the same extent as **11**, is significantly less able to affect the catalytic dyad (see yellow distance distribution in Figure 8), and along the trajectory, it moves away from the central position of *P2* reaching exposure to the bulk of the solvent at the end of the simulation.

Finally, compounds **62** and **181** behave similarly but neither of them reaches **11** and **179** destabilizing effects. Nevertheless, compound **62**, pushing with the quinoline against Trp207 and with the hydroxyl group against the backbone of Lys5, is the most impacting on Arg4-Glu290 with the highest value of 9.7 Å. The aromatic ring of **181** moves away around 6A from Arg4 finding accommodation at the center of *P2*, and all the hydrogen bond donors of the molecule chelate the carboxylic group of Glu288 from the beginning of the simulation to the end.

A global parameter reporting on the stability of the dimer interface can be calculated by measuring the pair distance fluctuations between one monomer and the other (see Methods): for every residue pair, with one residue of monomer A and the other of monomer B, their distance fluctuation over the MD trajectory measures their rigid coordination, and the average value over every A-B pair residue yields a global monomer−monomer coordination parameter.

Overall, most ligands induce a higher mean fluctuation when compared to the apo system, pointing to a reduced monomer−monomer coordination (Figure 9), with a larger effect for ligands in pocket *P2*. Therefore, compounds **11** and **179** cause the highest degree of fluctuations in the dimer. Compounds **177** and **181** follow. **62** falls behind all of them, with the lowest average of induced fluctuations, even though it was the highest-ranking compound in the docking score (see Table S2 in the Supporting Information).

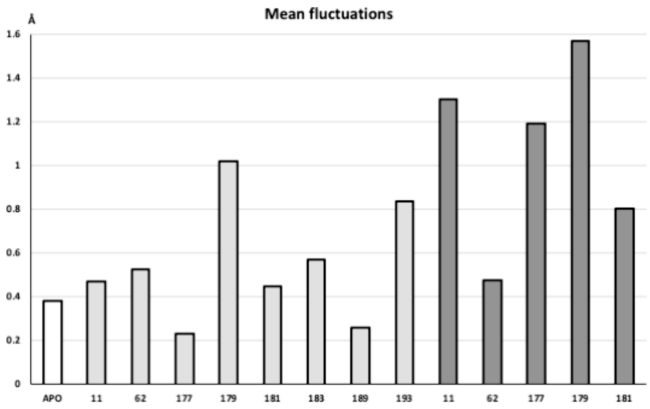

Figure 9. Global mean fluctuations of monomer−monomer pairwise amino acids (Å) for each complex. Apo in white, *P1*-ligand complexes in light gray, and *P2*-ligand complexes in dark gray.

Interestingly, **179** also impacts the coordination when bound to *P1*, together with **193**, while the other *P1* complexes appear to have a less significant effect on the monomer−monomer coordination.

Finally, to understand the source of the dimer stability modulation, the profile of protein internal mobility per residue can be mapped to highlight the localization of the perturbation between complexes and apo (Figure S4 in the Supporting Information). Ligands inducing higher monomer−monomer fluctuations like **179** and **11** on *P2* and **193** typically increase the mobility of loops 40−60 where His41 is located. This correlates with the local perturbation observed for the catalytic distance (yellow distributions in Figures 7 and 8).

Based on their predicted possible binding to the proximal site pocket *P1*, and the modeled effect on specific distances reporting on dimerization, a subset of compounds including **11**, **62**, **179**, **189**, and **193** was selected for subsequent testing.

According to our model, for these isoxazoline derivatives, proteolytic activity could be disrupted acting on both local dimerization stability (impairing the fundamental salt bridge between Arg4 and Glu290) and catalytic state (inducing variations in the relative position of the aiding His41 and the catalytic Cys145 and contributing to keeping the C-loop in the inactive conformation). The average impact on the dimerization distance for *P1* is reported in the SI.

On the other hand, ligands **11**, **177**, **179**, and **181**, when modeled in *P2*, also display an effect on global dimerization stability (see Figure 9) as well as some impact on the catalytic dyad (see Figure 8). The average impact on the catalytic distance for *P2* is reported in the SI. Hence, putting together the local perturbation analysis on key distances and the overall

https://doi.org/10.1021/acsomega.4c05480
ACS Omega 2024, 9, 41599−41615

dimerization stability in either putative binding pocket, compounds **11**, **179**, **189**, **193**, **62**, **177**, and **181** were selected for in vitro testing.

Chemistry. The compounds **11**, **62**, **177**, **179**, **181**, **183**, **189**, and **193**, whose structures are reported in Figures 5 and 6, were synthesized according to the procedures hereby described and relying upon chemical approaches sketched in Scheme 1.[26,27] Although synthesized, compound **183** has been discarded from in vitro tests for the reasons previously reported.

Quinoline Derivatives. Compound **62** is a known aminol prepared according to previously reported procedures, standing upon the 1,3-dipolar cycloaddition of *in situ*-generated quinolinenitrile oxide from the corresponding hydroxymoyl chloride **2** in the presence of triethylamine as a base and the *N*-benzoyl-2,3-oxazanorborn-5-ene **3** as dipolarophile (Scheme 2).[28]

Scheme 2. Synthetic Pathway toward Compound 62

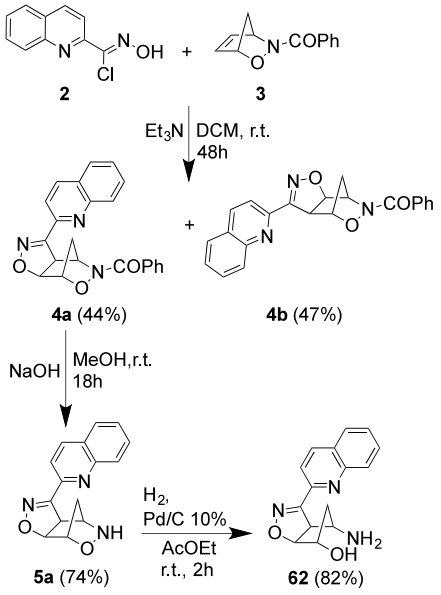

The regioisomeric cycloadducts **4a,b** were isolated, and only the syn isomer was submitted to subsequent alcoholysis, affording the hydroxylamine **5a**. The reductive cleavage of the N−O bond in compound **5a** afforded compound **62**.

p-Chloro Derivatives. The *N*-benzoyl-2,3-oxazanorborn-5-ene **3** was allowed to react with a slight excess (1.2 equiv) of 4-chloro-benzhydroxymoyl chloride **6**, in the presence of Et_3N, in a DCM solution for 2 days. The two regioisomeric cycloadducts **7a,b** were obtained and isolated in 48% and 45% yields, respectively (Scheme 3). Their structures relied on the basis of the corresponding analytical and spectroscopic data. The ^1H NMR spectrum ($CDCl_3$) of **7a** showed isoxazoline proton H5 at δ = 5.04 ppm (d, J = 8 Hz), coupled with the H4 proton at δ = 4.32 ppm (d, J = 8 Hz). Similarly, the proton spectrum of regioisomer **7b** showed the isoxazoline proton signal H5 at δ = 5.22 ppm (d, J = 8 Hz), coupled with the H4 proton at δ = 4.21 ppm (d, J = 8 Hz). The aromatic protons are clearly shown with a typical AA'BB' spin system in the expected range of chemical shifts.

The following synthetic steps run again through the classical pathway (see Notes) as we have shown in previous works[16] with few adaptations and experimental improvements. Alkaline

Scheme 3. Syntheses of Regioisomeric Aminols 177 and 193

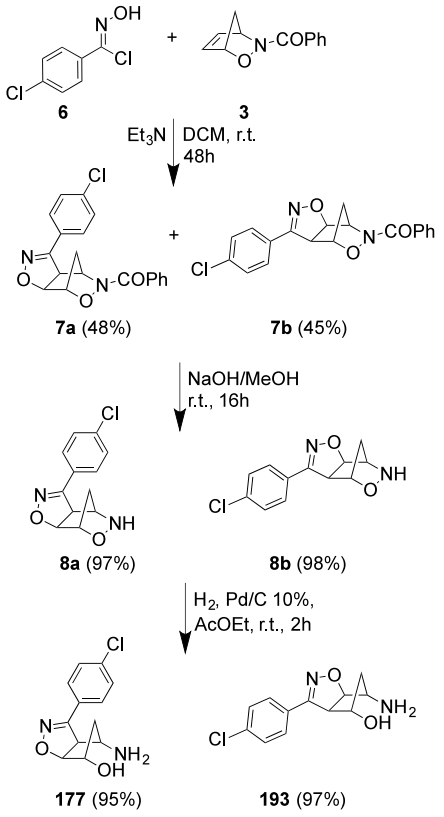

hydrolysis of the cycloadducts **7a,b**, conducted with ground NaOH in methanol solutions, afforded the corresponding hydroxylamine derivatives **8a,b** in nearly quantitative yield (Scheme 3).[17,18]

The ^1H NMR spectra ($CDCl_3$) of products **8a** and **8b** showed the absence of the proton signals corresponding to the benzoyl group. The relative IR spectra showed bands at ν_{NH} = 3209 cm^{-1} and ν_{NH} = 3243 cm^{-1}, respectively for **8a** and **8b**, corresponding to the NH group. Hydrogenolysis of the hydroxylamine derivatives under standard conditions (H_2, Pd/C 10%, AcOEt) afforded the desired aminols **177** and **193** (95 and 97% yields, respectively). The structures of **177** and **193** were confirmed from their analytical and spectroscopic data. In particular, the ^1H NMR spectra ($CDCl_3$) displayed a more complex fine structure with couplings due to the increased conformational mobility of the cyclopentane moieties following strain relief after hydrogenolytic ring opening. Significantly, the NH_2 and OH groups IR spectra furnished bands at ν_{NH2} = 3336 cm^{-1}, 3280 cm^{-1} and ν_{OH} = 3041 cm^{-1} for compound **177** while for compound **193** the corresponding groups gave stretching bands at ν_{NH2} = 3347 cm^{-1}, 3284 cm^{-1} and ν_{OH} = 3094 cm^{-1}.

Compound **177** was further elaborated through established procedures that quickly allowed the obtainment of the glycine derivatives **181** and **189** (Scheme 4).[29] The main steps involved OH protection and coupling with Fmoc-Gly-OH followed by removal of both protecting groups affording compound **181**. The intermediate amine **9** was obtained in 82% yield and the absence of the OH band in the IR spectrum confirmed its successful protection while in the ^1H NMR spectra ($CDCl_3$) the protons belonging to the *tert*-butyl-dimethyl silyl group appeared at δ = 0.15−0.93 ppm.

https://doi.org/10.1021/acsomega.4c05480
ACS Omega 2024, 9, 41599−41615

Scheme 4. Syntheses of the Glycine Derivatives 181 and 189

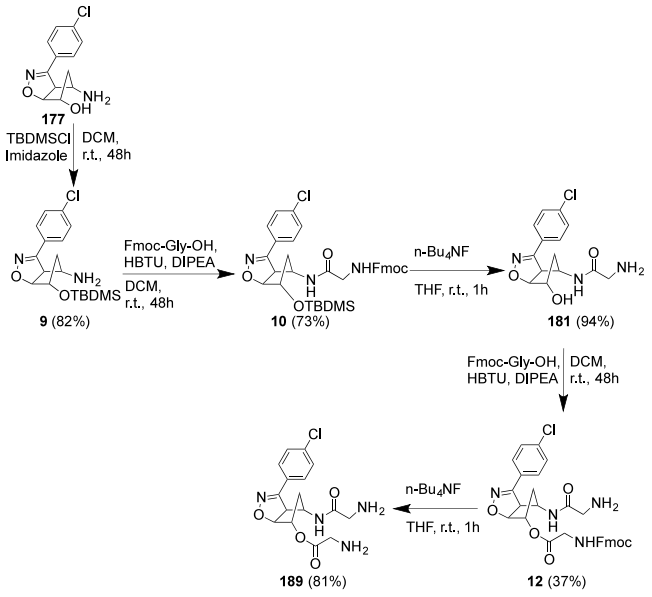

Scheme 5. Synthesis of Compound 179

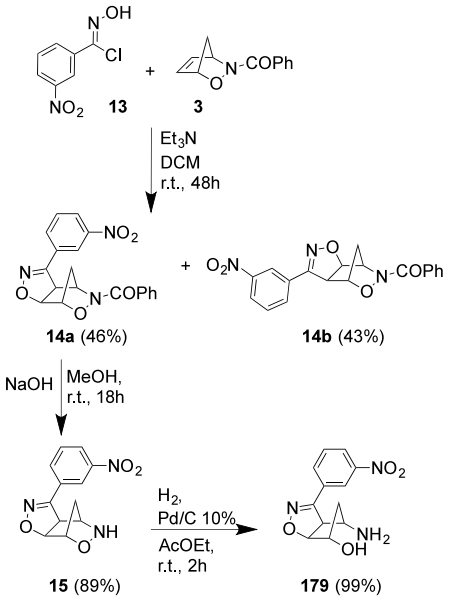

The amine **9** was then coupled with the commercially available Fmoc-Gly-OH and the adduct **10** was isolated in good yields (73%) and fully characterized. Fmoc signals crowded the aromatic region of the ^{1}H NMR spectra (DMSO-d_6), and the IR spectra displayed two carbonyl stretching peaks at ν_{CO} amide = 1681 cm^{-1} and ν_{CO} ester = 1703 cm^{-1}.

The hydroxy functionality deprotection was secured by standard *n*-Bu$_4$NF treatment; during this step, the Fmoc protection is also removed without detrimental effects in the subsequent synthetic step leading to the obtainment of compound **181** in good yields (88%). The Fmoc and TBDMS signals disappeared from the ^{1}H NMR spectra (DMSO-d_6) while the IR signals mutated from the sharp signals of NH groups to a broad band peaking at ν = 3310 cm^{-1} comprehending all signals of the groups OH NH and NH$_2$.

Starting from compound **181**, the Fmoc-Gly-OH coupling procedure (leading to the intermediate **12**) followed by removal of the protecting group afforded compound **189** (Scheme 4).

The intermediate **12** was obtained in fair yields (37%); the appearance in the ^{1}H NMR (DMSO-d_6) of Fmoc signals in the aromatic region of the spectrum as well as the glycine methylene CH_2-NHCO confirmed the assigned structure, together with the disappearance of the broad signal of the OH group from the IR. Fmoc removal with *n*-Bu$_4$NF treatment led to the obtainment of the target compound **189** in good yields (81%). Fmoc signals were no longer present in the ^{1}H NMR spectra (DMSO-d_6) and coherently was instead appreciable the broad signal at δ = 3.35 ppm, integrating for four protons, indicating NH$_2$ groups. The IR spectra accordingly displayed a broad band peaking at ν = 3235 cm^{-1} comprehending signals of groups NH and NH$_2$.

m-Nitro Derivatives. The *N*-benzoyl-2,3-oxazanorborn-5-ene **3** was allowed to react with the 3-nitro-benzonitrile oxide *in situ* generated from the corresponding hydroxymoyl chloride **13** in the presence of triethylamine as a base according to the known procedure in DCM solution for 2 days (Scheme 5). After this period of time, the residue, obtained after evaporation of the solvent, was submitted to chromatographic separation to isolate the two regioisomeric cycloadducts **14a** and **14b** in 43% and 46% yields, respectively.

Their structures were confirmed on the basis of their analytical and spectroscopic data. The ^{1}H NMR spectrum (CDCl$_3$) of **14a** showed the isoxazoline proton H5 at δ = 5.13 ppm (d, J = 8 Hz), coupled with the H4 proton at δ = 4.40 ppm (d, J = 8 Hz). Similarly, the ^{1}H NMR spectrum (CDCl$_3$) of regioisomer **14b** showed isoxazoline proton signal H5 at δ = 5.30 ppm (d, J = 8 Hz), coupled with the H4 proton at δ = 4.28 ppm (d, J = 8 Hz). In both cycloadducts, the aromatic protons are clearly shown in the ^{1}H NMR spectra (CDCl$_3$) with a series of deshielded signals in the expected range and also the IR band of the nitro group was observed at ν_{NO2} = 1521 cm^{-1}.

The hydrolytic detachment of the benzoyl group from cycloadduct **14a** was secured through alkaline hydrolysis, which took place in the presence of 1.7 equiv of NaOH in methanol, stirring at room temperature for 18 h. The hydroxylamine derivatives **15** was obtained in 89% yield, and fully characterized. The ^{1}H NMR spectra (CDCl$_3$) show the absence of the aromatic ring and the presence of a broad signal at δ = 4.79 originating from the NH proton. The NH group is also clearly shown in the IR spectrum with a band at ν_{NH} = 3235 cm^{-1}. Hydrogenolysis of derivatives **15** under standard conditions (H$_2$, Pd/C 10%, EtOAc) afforded the desired aminol **179** in high yields of 99%. The structure was established on the basis of their analytical and spectroscopic data. In particular, in the ^{1}H NMR (CDCl$_3$) spectra the isoxazoline signals were not affected by hydrogenation: δ = 4.01 (d, J = 8 Hz, H4), 5.39 ppm (d, J = 8 Hz, H5). Cleavage of the bicycle [2.2.1] ring affords the OH and NH$_2$ groups on the cyclopentane spacer, giving broad signals in the proton spectrum (CDCl$_3$) at δ = 5.15 ppm, while the corresponding bands were pretty evident in the IR spectra at ν_{NH2} = 3358 cm^{-1}, 3291 cm^{-1} and ν_{OH} = 3086 cm^{-1}.

Compound **179** was further elaborated through the previously reported procedure to synthesize compound **183** (Scheme 6).

The hydroxy group protection was performed under a standard method affording the amine **16** (57%) that was fully

https://doi.org/10.1021/acsomega.4c05480
ACS Omega 2024, 9, 41599−41615

Scheme 6. Synthesis of Compound 183

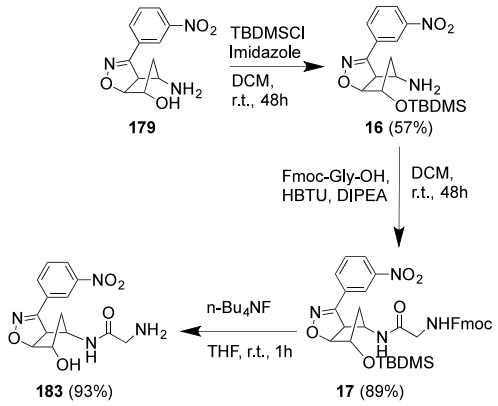

Scheme 7. Synthesis of Compound 11

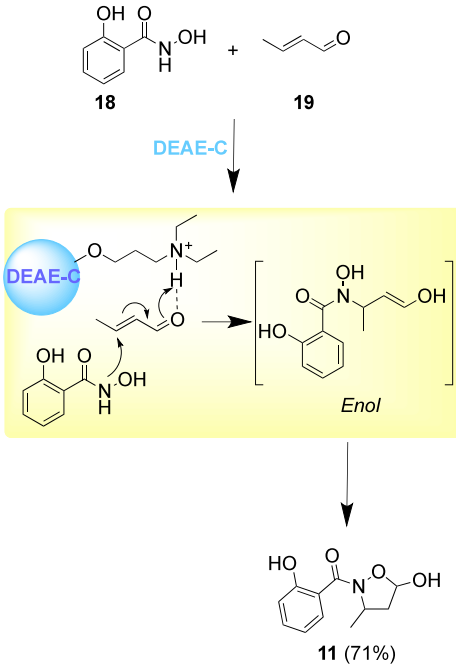

characterized. The appearance of shielded proton signals in the ^{1}H NMR spectra ($CDCl_3$) at δ = 0.11−1.03 ppm confirmed the presence of the *tert*-butyl-dimethyl silyl group and the absence of the OH band in the IR spectra corroborated the assigned structure. Compound **16** was then coupled with the commercially available Fmoc−Gly−OH and the adduct **17** was isolated in fair yields (89%). Fmoc signals crowded the aromatic region of the ^{1}H NMR spectra ($CDCl_3$), and the IR spectra displayed two carbonyl stretching peaks at ν_{CO} amide = 1722 cm^{-1} and ν_{CO} ester = 1674 cm^{-1}.

The hydroxy functionalities deprotection was secured by standard *n*-Bu_4NF treatment; during this step, the Fmoc protection was also removed leading to the obtainment of compound **183** in good yields (93%). The Fmoc and TBDMS signals disappeared from the ^{1}H NMR spectra (DMSO-d_6) and the OH group was evident at δ = 5.77 ppm. The aminol broad IR bands were found at ν_{NH2} = 3343 cm^{-1}, 3295 cm^{-1}; ν_{OH} = 3086 cm^{-1}.

5-Hydroxy Isoxazolidine Derivative. For the synthesis of the 3-methyl-5-hydroxy-isoxazolidine **11**, a catalytic method was preferred to the classical ene addition of nitrosocarbonyl intermediate, obtaining the desired compound in higher yields (Scheme 7).

The protocol[20,30] involves the use of diethylaminoethyl cellulose (DEAE-C) conducting the reaction in the solid state with by grinding/mixing in a mortar the hydroxamic acid **18** and the α,β-unsaturated aldehyde **19**. The 5-hydroxy-substituted isoxazolidine **11** was hence obtained in good yields (71%).

The isoxazolidine **11** was characterized and resulted identically in an authentic sample previously synthesized and available in our laboratory.

Biological Assays. Samples of the synthesized compounds, representative of the two nitrosocarbonyl families, isoxazoline-cyclopentane aminols and 5-hydroxy-isoxazolidine, i.e., compounds **11**, **62**, **177**, **179**, **181**, **189**, and **193**, were biologically assayed to preliminarily assess their potential as antiviral compounds capable of inhibiting SARS-CoV-2 NSP5 protease.

To this purpose, first, their cytotoxicity was assayed in terms of inhibition of cell metabolic activity in epithelial HepG2 cells. The test compounds were initially dissolved in DMSO at the final concentration of 40 mM and the exponentially growing cells were seeded into a 96-well flat bottom plate and incubated at 37 °C. After 24 h, the medium was replaced with fresh medium containing different concentrations of test compounds or the same volume of DMSO diluent (vehicle control). All samples were incubated for a further 24 h, and cell metabolic activity was detected by the MTS assay (Cell Titer 96 Aqueous One Solution, Promega, Madison, WI, USA) according to standard procedures. Cytotoxicity was then calculated as the concentration of the compounds needed to reduce the metabolic activity by 50% with respect to control cells (CC_{50}).

Figure 10 reports the metabolic activity assessed by the MTS assay in HepG2 cells treated with the potential NSP5 inhibitor selected compounds and related CC_{50} values.

Results showed that compounds **62**, **177**, and **179** were endowed with a higher ability to reduce the cell metabolic activity toward the cell line tested compared to the other compounds. Among the remaining group of compounds,

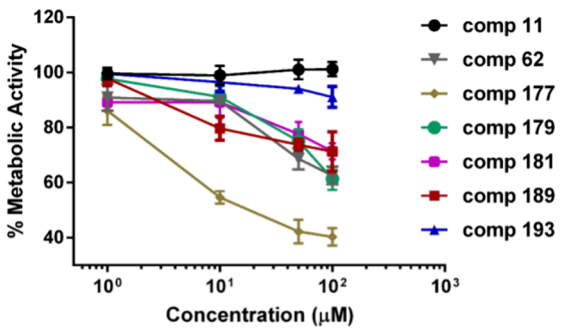

	Compounds						
	11	62	177	179	181	189	193
CC_{50} (μM)	> 1000	141.0 ± 9.2	29.9 ± 0.4	157.6 ± 7.4	202.9 ± 8.9	213.7 ± 4.5	986.1 ± 0.8

Figure 10. Evaluation of the metabolic activity assessed by the MTS assay in HepG2 cells treated with the potential NSP5 inhibitors for 24 h and related CC_{50} values. Data are expressed as % metabolic activity with respect to mean vehicle control value and refer to three experiments performed in duplicate.

https://doi.org/10.1021/acsomega.4c05480
ACS Omega 2024, 9, 41599−41615

compounds **181** and **189** were also endowed with a certain ability to reduce the cell metabolic activity with respect to compounds **11** and **193** that showed higher CC_{50} values. Nevertheless, the CC_{50} values of compounds **181** and **189** toward HepG2 cells were above 200 μM, i.e., a relatively high value, indicating that none of this group of compounds displayed high levels of cytotoxicity.

To ascertain their actual inhibitory activity toward NSP5, all the compounds selected for the biological assays were then subjected to a preliminary screening to ascertain their potential NSP5-inhibitory activity at a fixed concentration of 100 μM. This concentration was chosen as the maximal concentration that, based on the results obtained in the cytotoxicity assays, could be considered to provide an acceptable selectivity index for the compounds under investigation. In these and other NSP5-inhibitory assays, GC-376, a broad-spectrum inhibitor of viral proteases, including NSP5 SARS-CoV-2 protease, was utilized as reference NSP5 inhibitor.[31]

Figure 11 reports the results of the inhibition of the NSP5 enzymatic activity, as determined by the FRET assay. As clearly shown, compounds **62**, **177**, **179**, and **181** did not exert any significant reduction in viral protease activity, even at the high concentration assayed. Compounds **193**, **189**, and **11**, in different, induced a statistically significant inhibition of the NSP5 enzymatic activity. Consequently, only this subgroup of compounds was subjected to a more detailed, dose-dependent screening to determine their IC_{50} values, indicating their inhibitory potential by achieving a 50% reduction in the measured NSP5 protease activity (Figure 12).

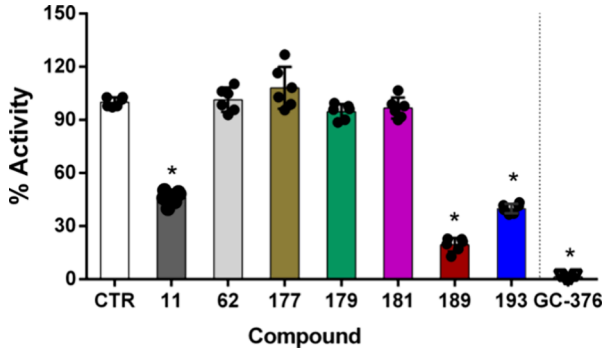

Figure 11. Screening of the compounds against SARS-CoV-2 NSP5 protease enzymatic activity using an FRET assay. Data are expressed as % activity with respect to mean control diluent value and refer to the fixed concentration assayed of 100 μM. GC-376 was used as reference NSP5 inhibitor at the fixed concentration of 50 μM. The asterisk denotes statistical significance, with p*< 0.0001, indicating significant differences compared to vehicle control sample (CTR).

As shown in Figure 12 compound **189** showed an IC_{50} mean value of 19.7 μM, remarkably lower than those of compounds **11** (75.0 μM) and compound **193** (55.8 μM). Moreover, the IC_{50} value of compound **189** was quite lower than its CC_{50} value, indicating a good selectivity index.

Overall, the results of the biological assays experimentally confirmed what was predicted by the computational analysis about the capability of a few of the synthesized compounds to efficiently interact with the functional activity of SARS-CoV-2 NSP5 protease. On the other hand, the results indicated that the currently designed structures of the compounds are also endowed with a certain cytotoxic potential. Nevertheless, results obtained with compound **189** are encouraging.

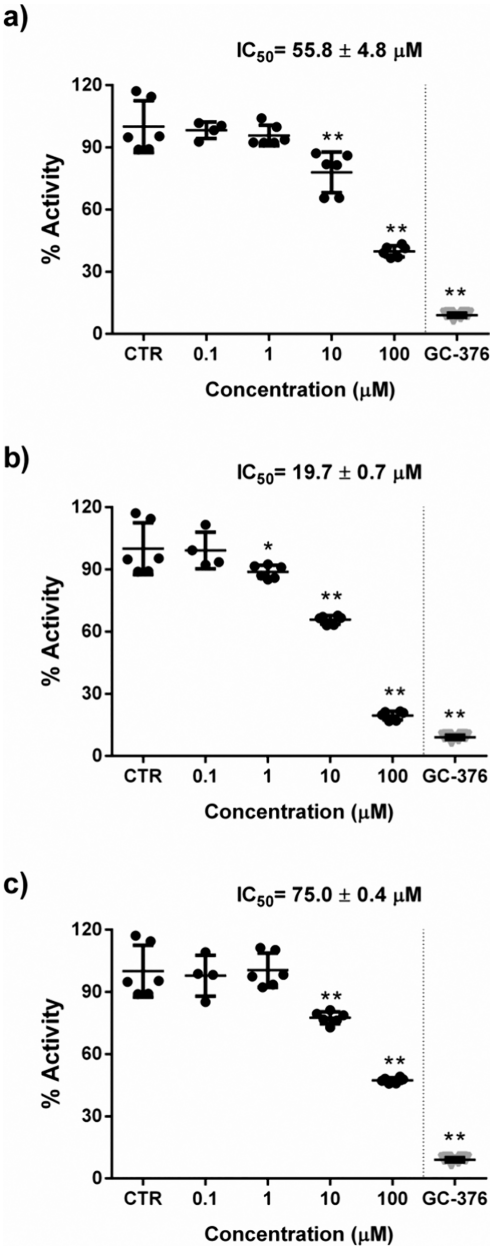

Figure 12. Screening of compounds **193** (a), **189** (b), and **11** (c) against SARS-CoV-2 NSP5 protease enzymatic activity using a FRET assay. Data are expressed as % activity with respect to the mean vehicle control value. Calculated IC_{50} values for each compound are also reported. GC-376 was used as reference NSP5 inhibitor at the fixed concentration of 50 μM. Asterisks denote statistical significance, with p*< 0.05 and p**< 0.0001 indicating significant differences compared to vehicle control sample (CTR).

DISCUSSION AND CONCLUSIONS

In the present work, we have designed and synthesized potential NSP5 allosteric inhibitors exploiting both MD data on SARS-CoV-2 and the chemical protocols developed by the Pavia research group.[15] The protease is a dimer in solution because of the stable pairing of extremely conserved motifs, some of which could become good targets. Clustering analysis on Cα assisted by SiteMap runs to rank the putative binding sites on the protein surface led us to identify the most druggable allosteric pockets of SARS-CoV-2 NSP5 protease. The comparison between our findings and those reported in

https://doi.org/10.1021/acsomega.4c05480
ACS Omega 2024, 9, 41599−41615

the literature led us to validate our selection of allosteric sites whose regulation (perturbation) may be able to impact protein−protein interactions and destabilize the active site.[6,7,14] Furthermore, a second clustering analysis focusing on the side chains that define the pockets was fundamental to obtaining receptor conformations that are suited for the drug design phase. We then created a database of differently decorated scaffolds to be computationally evaluated for their potential inhibitory activity. The docking screening was the first step in the selection of candidate molecules to be synthesized.

The accordance between MD simulations of our ligand−protein modeled complexes confirmed the consistency of our strategy. The computational studies revealed the possibility for two recurring scaffolds, namely, the cyclopentane-fused isoxazolines and the isoxazolidines, giving positive responses in terms of inhibiting SARS-CoV-2 NSP5. At the head of former scaffold group, we found mostly aminols in forms of compounds **62**, **177**, **179**, and **193**. Compounds **181** and **189** expanded this group including mono- or bisubstituted glycine isoxazoline derivatives. The last scaffold was represented by 5-hydroxy isoxazolidine derivative **11**. In principle, these compounds could recognize allosteric NSP5 sites and interact with sites other than those occupied by Nirmatrelvir (Paxlovid) and other peptidomimetics.

In this POC study, the reported synthetic pathway toward targeted compounds found a robust and reliable method in the well-documented 1,3-dipolar cycloaddition reactions of suitable nitrile oxides toward a highly reactive dipolarophile, the *N*-benzoyl-2,3-oxazanorborn-5-ene **3** derived from the chemistry of nitrosocarbonyl intermediates. These cycloaddition reactions often provided a unique opportunity to use valuable building blocks allowing introduction of different aromatic or heterocyclic substituents, with variable stereochemistry, bearing different functional groups.[15,16] Single or double amino acid residues were introduced on the selected aminols through a well-established and straightforward chemistry.[29] In terms of yields, all the synthetic steps gave from fair to optimum results, and the quality of the products was found to be encouraging. The use of an unconventional absorbent based on cellulose (DEAE-C) was finally proposed to take advantage of the cyclization of hydroxamic acids on unsaturated aldehydes for the preparation of the 5-hydroxy-isoxazolidines in good yields and, more intriguingly, in an extremely mild way at room temperature and in the solid phase.[20,30]

These two goals cannot stand on a solid plane unless verified on a biological ground (Figure 13).

The biological assays experimentally somewhat confirmed what was predicted by the computational analysis about the capability of a few of the synthesized compounds to efficiently interact with the functional activity of SARS-CoV-2 NSP5. Specifically, among the compounds showing a good docking score, our minimalistic model based on the level of perturbation of two characteristic distances yields a putative activity ranking. The compounds selected for site *P1* in particular are predicted to affect the dimerization of NSP5 via an increase of the average Arg4-Glu290 distance. Interestingly, 3 out of 6 selected putative ligands for this pocket show in vitro inhibitory activity, and the activity correlates with the average Arg4-Glu290 distance increase. This supports our mechanistic model. On the other hand, compound **11** is also compatible with binding to *P2*, where it might affect the stability of the dimer, as suggested by the distance fluctuation analysis.

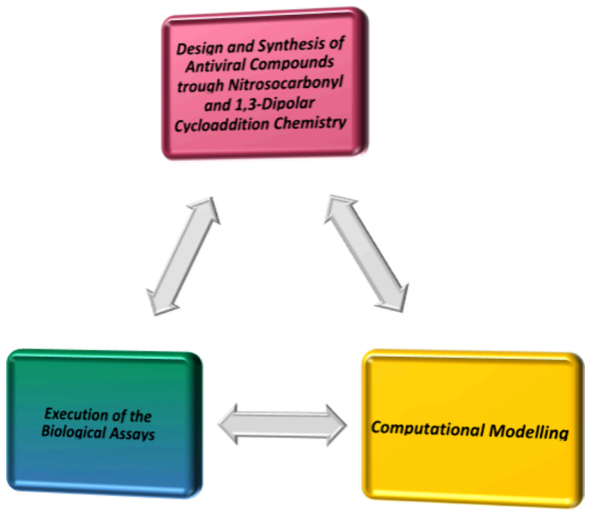

Figure 13. Pivotal combination of the three pillars [*modeling*⇔*chemistry*⇔*in vitro tests*].

Further structural studies will be needed to validate the binding site and the inhibitory mechanism of this ligand. Among the tested molecules, compound **189** has shown a quite good selectivity index (SI = 10.85), exhibiting an encouraging, potential antiviral activity for possible derivative compounds. Of course, an important limitation of the study, as far as biological activity is concerned, is represented by the fact that viral infection assays have not been carried out. However, as repeatedly specified above, this biological preliminary phase focused on the experimental ascertainment that at least some of the compounds for which the *in silico* studies had predicted the ability to interact with allosteric sites of NSP5 were indeed able to inhibit the enzymatic activity of the viral protein and had limited cytotoxic activity. Future studies, aimed at identifying the real antiviral activity of the compounds, will examine the infectious aspects in detail. On the other hand, the results indicated that the currently designed structures of the compounds are also endowed with a certain but, except for compound **177**, quite low cytotoxic potential.

This drawback must be taken into account in relationship with the use of the proposed synthetic protocol as the strategic way to select the candidates for the SARS-CoV-2 protease inhibition, but nothing is precluded for testing the compounds here presented or others against enzymes belonging to those respiratory viruses that recently have been pointed out as relevant candidates for antiviral compound discovery plan.

In conclusion, this investigation promises a good advancement in the battle against SARS-CoV-2 by unveiling a strategic approach that seamlessly integrates computational analyses, synthetic chemistry, and biological assays. The discovery of allosteric pockets within the SARS-CoV-2 NSP5 protease, achieved through computational methods and corroborated by literature data, has illuminated a promising avenue for targeted antiviral intervention.[6−14] The subsequent design and synthesis of novel antiviral molecules, harnessing the distinctive chemistry developed by our research group, showcase a pioneering effort in structure-based drug design. As a matter of fact, identifying and focusing on allosteric sites can lead to the discovery of new therapeutic classes and the expansion of lead compound chemical space. The identification of novel compounds that target allosteric regions offered a workable approach to the quest for novel inhibitors of PP interactions.

https://doi.org/10.1021/acsomega.4c05480
ACS Omega 2024, 9, 41599−41615

Our goal though was to find active hits by employing data on an allosteric pocket that we directly gathered from the analysis of a dynamic molecular machine. As we navigate the dynamic landscape of viral infections, the collaborative synergy between computational efforts, synthetic chemistry, and biological tests emphasizes the importance of a holistic approach. The deliberate exploitation of pericyclic reactions, ultimately in the form of 1,3-dipolar cycloadditions[32] and catalyzed methods in the synthetic process adds a layer of renewal and originality, enabling the "creation" of compounds with tailored structures designed to interact specifically with the identified allosteric sites. With this approach, we not only demonstrated the versatility of the presented chemistry, but we also highlighted its utility in crafting molecules with enhanced potential antiviral properties. The successful translation of computational insights into tangible antiviral candidates underscores the efficacy of this multidisciplinary strategy.[33]

EXPERIMENTAL SECTION

General. All melting points (mp) are uncorrected. ^{1}H and ^{13}C NMR spectra were recorded on 300 and 400 MHz spectrometers (solvents specified). Chemical shifts are expressed in ppm from internal tetramethylsilane (δ) and coupling constants (J) are in Hertz (Hz): b, broad; s, singlet; bs, broad singlet; d, doublet; t, triplet; q, quartet; m, multiplet. IR spectra (ATR) were recorded on an Agilent Technologies Cary 630 ZnSe Engine spectrophotometer available at the Department, and absorptions (ν) are in cm^{-1}. HRMS were done on an X500B QTOF system (Sciex, Framingham, MA 01701 USA) available at the CGS of the University of Pavia. Column chromatography and tlc: silica gel H60 and GF_{254}, respectively; eluants: cyclohexane/ethyl acetate 9:1 to pure ethyl acetate.

Starting and Reference Materials. Compounds **3**, **6**, **13**, and **62** were synthesized according to the procedure reported in the literature.[16−20,34] Other reagents and solvents were purchased from chemical suppliers and used without any further purification following or adapting the methods reported in the cited literature.

Synthesis of Cycloadducts 7a,b. *N*-Benzoyl-2,3-oxazanorborn-5-ene **3** (1.5 g, 7.5 mmol) was dissolved in anhydrous DCM (150 mL) along with triethylamine (1.25 mL, 9.0 mmol); a solution of 4-chloro-benzhydroximoyl chloride **6** (1.56 g, 8.2 mmol) in the same solvent (50 mL) was added dropwise under stirring at 0 °C over 2 h. After keeping the reaction for 2 days at room temperature, the organic phase was washed twice with water and dried with anhydrous Na_2SO_4. The filtrate was evaporated under reduced pressure leaving a residue that was submitted to column chromatography.

*Compound **7a**.* 1.27 g (48%), mp 154−155 °C from acetone.

IR: ν = 1632 (C═O), 1595 (C═N) cm^{-1}.

^{1}H NMR (400 MHz, DMSO-d_6, 25 °C): δ = 2.05 and 2.15 (m, 2H, CH_2), 4.32 (d, 1H, J = 8 Hz, $H4_{Isox.}$), 4.96 (s, 1H, CH-N), 5.04 (dt, 1H, J = 8, 1 Hz, $H5_{Isox.}$), 5.11 (s, 1H, CH−O), 7.43 (AA'BB' syst., 2H, arom.), 7.48 (AA'BB' syst., 2H, arom.), 7.58 (m, 1H, arom.), 7.70 (m, 2H, arom.), 7.85 (m, 2H, arom.).

^{13}C NMR (100 MHz, $CDCl_3$, 25 °C): δ = 32.7, 55.2, 58.5, 81.2, 83.0, 126.1, 128.1, 128.2, 129.1, 129.5, 132.3, 136.8, 154.5, 171.2.

$C_{19}H_{15}ClN_2O_3$ (354.79): HRMS: calcd (MW+Na) 377.0663; found 377.0657.

*Compound **7b**.* 1.19 g (45%), mp 129−130 °C from acetone.

IR: ν = 1651 (C═O), 1599 (C═N) cm^{-1}.

^{1}H NMR (400 MHz, DMSO-d_6, 25 °C): δ = 2.08 (m, 2H, CH_2), 4.21 (d, 1H, J = 8 Hz, $H4_{Isox.}$), 4.99 (s, 1H, CH-N), 5.15 (bs, 1H, CH−O), 5.22 (d, 1H, J = 8 Hz, $H5_{Isox.}$), 7.43 (d, J = 8 Hz, 2H, arom.), 7.47 (t, 2H, J = 8 Hz, arom.), 7.55 (t, 1H, J = 8 Hz, arom.), 7.67 (d, 2H, J = 8 Hz, arom.), 7.80 (d, 2H, J = 8 Hz, arom.).

^{13}C NMR (100 MHz, $CDCl_3$, 25 °C): δ = 32.7, 57.2, 61.9, 79.9, 83.0, 126.3, 127.9, 128.4, 128.8, 129.5, 132.1, 132.8, 136.9, 154.1, 170.4.

$C_{19}H_{15}ClN_2O_3$ (354.79): HRMS: calcd (MW+Na) 377.0663; found 377.0658.

Synthesis of hydroxylamines 8a,b. Cycloadducts **7a,b** (2.1 g, 5.9 mmol) were dissolved in MeOH (100 mL) and powdered NaOH (0.40 g, 10.1 mmol) was added portionwise at rt. The reaction mixture was stirred for 48 h. After this period of time, the solvent was evaporated at reduced pressure, the residue was taken up with DCM, and the organic phase was washed with brine and finally dried over anhydrous Na_2SO_4. Upon evaporation of the solvent, the crude solid products **8a,b** were collected, properly recrystallized, and fully characterized.

*Compound **8a**.* 1.44 g (97%), mp 148−149 °C from acetone-iPr_2O.

IR: ν = 3209 (NH), 1588 (C═N) cm^{-1}.

^{1}H NMR (400 MHz, DMSO-d_6, 25 °C): δ = 1.82 and 2.09 (m, 2H, CH_2), 4.00 (d, 1H, J = 8 Hz, $H4_{Isox.}$), 4.03 (s, 1H, CH-N), 4.71 (s, 1H, CH−O), 5.90 (d, 1H, J = 8 Hz, $H5_{Isox.}$), 7.42 (AA'BB' syst., 2H, arom.), 7.68 (AA'BB' syst., 2H, arom.).

^{13}C NMR (100 MHz, $CDCl_3$, 25 °C): δ = 35.0, 55.9, 59.2, 77.5, 84.0, 126.7, 128.0, 129.3, 136.5, 155.0.

$C_{12}H_{11}ClN_2O_2$ (250.68): HRMS: calcd (MW+H) 251.0582; found 251.0579.

*Compound**8b**.* 1.45 g (98%), mp 182−183 °C from acetone-iPr_2O.

IR: ν = 3243 (NH), 1592 (C═N) cm^{-1}.

^{1}H NMR (400 MHz, DMSO-d_6, 25 °C): δ = 1.84 and 2.11 (d, 2H, J = 16 Hz, CH_2), 3.98 (d, 1H, J = 8 Hz, $H4_{Isox.}$), 4.10 (s, 1H, CH-N), 4.73 (s, 1H, CH−O), 5.00 (d, 1H, J = 8 Hz, $H5_{Isox.}$), 7.41 (AA'BB' syst., 2H, arom.), 7.67 (AA'BB' syst., 2H, arom.).

^{13}C NMR (100 MHz, $CDCl_3$, 25 °C): δ = 34.7, 57.9, 61.6, 76.4, 84.4, 126.8, 128.0, 129.3, 136.5, 154.6.

$C_{12}H_{11}ClN_2O_2$ (250.68): HRMS: calcd (MW+H) 251.0582; found 251.0578.

Synthesis of aminols 177 and 193. Compounds **8a,b** (1.9 g, 7.6 mmol) were dissolved in EtOAc (65 mL) along with 0.4 g of C/Pd 10%, and the mixture was submitted to hydrogenation at rt. The reaction was left under stirring witha hydrogen stream until it absorbed 170 mL. After this, the solution was filtered and the solvent was evaporated to dryness. The crude solid products **177** and **193** were recrystallized and fully characterized.

*Compound **177**.* 1.44 g (97%), mp 148−149 °C from MeOH-iPr_2O

IR: ν = 3336, 3280 (NH_2), 3041 (OH), 1607 (C═N) cm^{-1}.

^{1}H NMR (400 MHz, DMSO-d_6, 25 °C): δ = 1.84 (m, 2H, CH_2), 3.81 (d, 1H, J = 6 Hz, CH-N), 4.02 (d, 1H, J = 8 Hz $H4_{Isox.}$), 4.43 (d, 1H, J = 6 Hz, CH−O), 5.29 (d, 1H, J = 8 Hz, $H5_{Isox.}$), 7.43 (AA'BB' syst., 2H, arom.), 7.65 (AA'BB' syst., 2H, arom.).

https://doi.org/10.1021/acsomega.4c05480
ACS Omega 2024, 9, 41599−41615

^{13}C NMR (100 MHz, $CDCl_3$, 25 °C): δ = 32.5, 57.2, 77.2, 92.4, 126.7, 127.9, 128.8, 128.9, 129.2, 130.1, 156.2.

$C_{12}H_{13}ClN_2O_2$ (152.70): HRMS: calcd (MW+H) 253.0738; found 253.0736.

Compound ***193***. 1.86 g (97%), mp 194−195 °C from acetone-iPr_2O.

IR: ν = 3347, 3284 (NH_2), 3094 (OH), 1580 (C═N) cm^{-1}.

^{1}H NMR (400 MHz, $CDCl_3$, 25 °C): δ = 1.85 (m, 2H, CH_2), 3.97 (m, 1H, CH-N), 4.29 (s, 1H, CH−O), 4.32 (d, 1H, J = 8 Hz, H4 Isox.), 5.04 (d, 1H, J = 8 Hz, H5 Isox.), 7.41 (AA'BB' syst., 2H, arom.), 7.74 (AA'BB' syst., 2H, arom.).

^{13}C NMR (100 MHz, $CDCl_3$, 25 °C): δ = 38.6, 59.1, 62.6, 78.0, 91.8, 127.0, 127.2, 128.2, 128.9, 129.2, 136.1, 155.6.

$C_{12}H_{13}ClN_2O_2$ (152.70): HRMS: calcd (MW+H) 253.0738; found 253.0735.

Protection of aminol 177. In a 100 mL flask, 1.40 g (5.5 mmol) of aminol **177** was dissolved in 50 mL of anhydrous DCM along with 0.83 mg (12.2 mmol) of imidazole. TBDMSCl (0.92 g, 6.1 mmol) was then added under stirring at room temperature, and the solution was left to react for 48 h. After this period of time, the solution was diluted with DCM and washed with brine (3 × 20 mL). The organic phase was dried over anhydrous Na_2SO_4. Upon evaporation of the solvent, the pale yellow oils relative to the protected compound **9** was obtained and fully characterized.

Compound ***9***. 1.67 g (82%), mp 83−84 °C from *n*-hexane

IR: ν = 3388 (NH_2), 1592 (C═N) cm^{-1}.

^{1}H NMR (300 MHz, $CDCl_3$, 25 °C): δ = 0.15 (s, 3H, CH_3), 0.17 (s, 3H, CH_3), 0.93 (s, 9H, tBu), 1.74 and 1.91 (m, 2H, CH_2), 2.21 (bs, 2H, NH_2) 3.46 (d, 1H, J = 6 Hz, CH-N), 4.02 (d, 1H, J = 9 Hz, $H4_{Isox.}$), 4.46 (d, 1H, J = 4 Hz, CH−O), 5.05 (d, J = 9 Hz, 1H, $H5_{Isox.}$), 7.39 (AA'BB' syst., 2H, arom.), 7.73 (AA'BB' syst., 2H, arom.).

^{13}C NMR (75 MHz, $CDCl_3$, 25 °C): δ = −5.0, 17.8, 25.7, 41.0, 58.6, 62.1, 78.8, 92.7, 127.3, 128.2, 129.0, 135.9, 156.9.

$C_{18}H_{27}ClN_2O_2Si$ (366.96): HRMS: calcd (MW+H) 367.1603; found 367.1598.

Synthesis of Compound 10. In a 250 mL flask, 1.20 g (3.3 mmol) of amine **9** was dissolved in 120 mL of anhydrous DCM along with 1.43 g (3.6 mmol) of HBTU and 2.3 mL of DIPEA. Fmoc-Gly-OH (0.97 g, 3.3 mmol) was then added under stirring at room temperature, and the solution was left to react for 48 h. After this period of time, the organic phase is washed with brine and dried over anhydrous Na_2SO_4. Upon evaporation of the solvent, oily residues were collected, and product **10** was isolated from column chromatography and fully characterized.

Compound ***10***. 1.54 g (73%), mp 75−76 °C from acetone.

IR: ν = 3396 (NH), 1703 (C═ O), 1681 (C═O), 1591 (C═N) cm^{-1}.

^{1}H NMR (300 MHz, DMSO-d_6, 25 °C): δ = 0.10 (s, 3H, CH_3), 0.12 (s, 3H, CH_3), 0.89 (s, 9H, tBu), 1.69 and 1.90 (m, 2H, CH_2), 3.62 (d, 2H, J = 6 Hz, CH_2NH), 4.26 (m, 6H, CHO, CHN, $H4_{Isox.}$, CH_2O, CHFmoc), 4.96 (d, 1H, J = 9 Hz, $H5_{Isox.}$), 7.34 (t, 2H, J = 7 Hz, arom.), 7.43 (t, 2H, J = 7 Hz, arom.), 7.50 (d, 2H, J = 8 Hz, arom.), 7.63 (t, 1H, NH), 7.72 (d, 2H, J = 7, 3 Hz, arom. and NH), 7.80 (d, 2H, J = 8 Hz, arom.), 7.90 (d, 2H, J = 7 Hz, arom.).

^{13}C NMR (75 MHz, DMSO-d_6, 25 °C): δ = −5.0, 17.8, 25.7, 43.9, 46.6, 52.6, 57.3, 65.8, 78.2, 92.3, 120.1, 125.2, 127.1, 127.2, 127.6, 128.8, 128.9, 134.6, 140.7, 143.7, 143.8, 156.4, 156.6, 168.3.

$C_{35}H_{40}ClN_3O_5Si$ (646.26): HRMS: calcd (MW+Na) 668.2318; found 668.2356.

Synthesis of Compound 181. To solution of the compound **10** (0.65 g, 1.0 mmol) in anhydrous THF (50 mL), a 1 M solution of *n*-$Bu_4N^+F^-$ (1.2 mL, 1.2 mmol) was added under stirring at room temperature. The mixture was left to stir for 1 h. Then, the solution was concentrated, taken up with DCM (150 mL), washed with brine (3 × 30 mL), and finally dried over Na_2SO_4. The crude solid product **181** was recrystallized and fully characterized.

Compound ***181***. 0.29 g (94%), mp 139−140 °C from acetone.

IR: ν = 3310−3050 (NH_2, OH), 1636 (C═O), 1592 (C═N) cm^{-1}.

^{1}H NMR (300 MHz, DMSO-d_6, 25 °C): δ = 1.71 (s, 2H, NH_2), 1.83 (s, 2H, CH_2), 3.75 (m, 2H, CH_2), 4.17 (d, 1H, J = 9 Hz, $H4_{Isox.}$), 4.29 (s, 1H, CH-N), 4.45 (m, 1H, CH−O), 5.02 (d, 1H, J = 9 Hz, $H5_{Isox.}$), 5.77 (d, 1H, J = 2 Hz, OH), 7.51 (AA'BB' syst., 2H, arom.), 8.01 (AA'BB' syst., 2H, arom.), 8.55 (d, 1H, J = 9 Hz, NHCO).

^{13}C NMR (75 MHz, DMSO-d6, 25 °C): δ = 29.0, 36.4, 53.4, 53.6, 59.7, 76.8, 91.8, 127.5, 128.8, 134.7, 155.7, 169.1, 169.4.

$C_{14}H_{16}ClN_3O_3$ (309.75): HRMS: calcd (MW+H) 310.0953; found 310.0961.

Synthesis of Compound 12. In a 250 mL flask, 0.30 g (1.0 mmol) of compound **181** was dissolved in 100 mL of anhydrous DCM. DIC (0.25 g, 2.0 mmol) was added along with a catalytic amount of DMAP and Fmoc-Gly-OH (0.32 g, 1.1 mmol) under stirring at room temperature, and the solution was left to react for 48 h. After this period of time, the organic phase is washed with a saturated solution $NaHCO_3$ and brine and dried over anhydrous Na_2SO_4. Upon evaporation of the solvent, an oily residue was collected and product **11** was isolated from column chromatography and fully characterized.

Compound ***12***. 0.21 g (37%), mp 123−124 °C from acetone-iPr_2O.

IR: ν = 3295 (NH_2), 1655 (C═O), 1595 (C═N) cm^{-1}.

^{1}H NMR (300 MHz, DMSO-d_6, 25 °C): δ = 1.80−2.10 (m, 2H+2H, CH_2 and CH_2NH_2), 2.90 (bs, 2H, NH_2), 3.17 (2H, CH_2NHCO), 3.41 (bs, 2H, CH_2O), 4.30 (d, 1H, J = 8 Hz, $H4_{Isox.}$) 4.37 (bs, 1H CHN), 5.01 (t, 1H, J = 3 Hz, CHFmoc), 5.18 (d, 1H J = 8 Hz, $H5_{Isox.}$), 5.23 (bs, 1H, CHO), 6.58 (d, 1H, J = 6 Hz, NHCO), 7.45 (m, 6H, arom.), 7.85 (m, 4H, arom.), 8.00 (d, 2H, J = 8 Hz, arom.), 8.11 (d, 1H, J = 6 Hz, NHCO).

^{13}C NMR (75 MHz, DMSO-d_6, 25 °C): δ = 26.3, 38.7, 53.5, 89.3, 106.7, 109.7, 120.0, 121.4, 127.1, 127.3, 128.9, 134.9, 137.4, 139.4, 142.6, 149.2, 154.0, 169.8, 171.9.

$C_{31}H_{29}ClN_4O_6$ (589.05): HRMS: calcd ($C_{16}H_{19}ClN_4O_4$+H) 367.1168; found 367.1169.

Synthesis of Compound 189. To solution of the compound **12** (0.28 g, 0.5 mmol) in anhydrous THF (50 mL), a 1 M solution of *n*-$Bu_4N^+F^-$ (0.48 mL, 0.5 mmol) was added under stirring at room temperature. The mixture is left under stirring for 1 h. Then the solution was concentrated, taken up with DCM (100 mL), washed with brine (3 × 20 mL), and finally dried over Na_2SO_4. The crude solid product **189** was recrystallized and fully characterized.

Compound ***189***. 0.14 g (81%), mp 153−154 °C from acetone-iPr_2O.

IR: ν = 3235 (NH_2, NH), 1655 (C═O), 1603 (C═N) cm^{-1}.

https://doi.org/10.1021/acsomega.4c05480
ACS Omega 2024, 9, 41599−41615

^{1}H NMR (300 MHz, DMSO-d_6, 25 °C): δ = 1.60 and 1.73 (m, 2H, CH_2), 3.17 (m, 2H+2H, CH_2), 3.35 (bs, 4H, NH_2), 4.13 (d, 1H, J = 8 Hz, $H4_{Isox.}$), 4.97 (d, 1H, J = 8 Hz, $H5_{Isox.}$), 5.17 (bs, 1H, CHN), 5.19 (bs, 1H, CHO), 7.49 (AA'BB' syst., 2H, arom.), 7.88 (AA'BB' syst., 2H, arom.), 8.90 (b, 1H, NH).

^{13}C NMR (75 MHz, DMSO-d_6, 25 °C): δ = 30.4, 57.49, 57.5, 58.5, 76.8, 77.6, 92.6, 127.5, 128.7, 128.8, 134.5, 156.1, 167.4, 173.7.

$C_{31}H_{29}ClN_4O_6$ (366.80): HRMS: calcd (MW+H) 367.1168; found 367.1169.

Synthesis of Cycloadducts 14a,b. *N*-Benzoyl-2,3-oxaza-norborn-5-ene **3** (2.0 g, 9.9 mmol) was dissolved in anhydrous DCM (150 mL) along with triethylamine (1.66 mL, 11.9 mmol); a solution of 3-nitro-benzhydroximoyl chloride **13** (1.56 g, 8.2 mmol) in the same solvent (50 mL) was added dropwise under stirring at 0 °C over 2 h. After keeping the reaction for 2 days at room temperature, the organic phase was washed twice with water and dried with anhydrous Na_2SO_4. The filtrate was evaporated under reduced pressure leaving a residue that was submitted to column chromatography.

Compound ***14a***. 1.67 g (46%), mp 173−174 °C from acetone.

IR: ν = 1614 (C═O), 1595 (C═N), 1521 (NO_2) cm^{-1}.

^{1}H NMR (300 MHz, $CDCl_3$, 25 °C): δ = 2.04 (d, 1H, J = 12 Hz, CH_2), 2.15 (dd, 1H, J = 12, 5 Hz, CH_2) 4.40 (d, 1H, J = 8 Hz, $H4_{Isox.}$), 5.00 (s, 1H, CH-N), 5.12 (s, 1H, CH−O), 5.13 (d, 1H, J = 8 Hz, $H5_{Isox.}$), 7.50 (m, 3H, arom.), 7.67 (t, 1H, J = 8 Hz, arom.), 7.86 (d, 2H, J = 8 Hz, arom.), 8.10 (d, 1H, J = 8 Hz, arom.), 8.32 (d, 1H, J = 8 Hz, arom.), 8.61 (s, 1H, arom.).

^{13}C NMR (75 MHz, $CDCl_3$, 25 °C): δ = 32.6, 54.9, 58.9, 80.8, 83.6, 121.3, 125.0, 128.3, 128.9, 129.4, 130.3, 132.2, 132.4, 148.6, 153.8, 171.4.

$C_{19}H_{15}N_3O_5$ (365.35): HRMS: calcd (MW+H) 366.1084; found 366.1071.

Compound ***14b***. 1.56 g (43%), mp 157−158 °C from acetone.

IR: ν = 1638 (C═O), 1599 (C═N), 1517 (NO_2) cm^{-1}.

^{1}H NMR (300 MHz, $CDCl_3$, 25 °C): δ = 2.13 (m, 2H, CH_2), 4.28 (d, 1H, J = 8 Hz, $H4_{Isox.}$), 5.04 (s, 1H, CH-N), 5.22 (s, 1H, CH−O), 5.30 (d, 1H, J = 8 Hz, $H5_{Isox.}$), 7.49 (m, 2H, arom.), 7.57 (m, 1H, arom.), 7.67 (t, 1H, J = 8 Hz, arom.), 7.81 (m, 2H, arom.), 8.11 (d, 1H, J = 8 Hz, arom.), 8.32 (m, 1H, arom.), 8.54 (s, 1H, arom.).

^{13}C NMR (75 MHz, $CDCl_3$, 25 °C): δ = 32.7, 56.7, 77.1, 79.6, 83.6, 121.3, 125.0, 128.3, 128.8, 129.6, 130.2, 132.0, 132.1, 132.5, 148.6, 153.4, 170.6.

$C_{19}H_{15}N_3O_5$ (365.35): HRMS: calcd (MW+H) 366.3533; found 366.3537.

Synthesis of Aminol 15. Compound **14a** (1.35 g, 3.7 mmol) was dissolved in MeOH (100 mL), and powdered NaOH (0.25 g, 6.3 mmol) was added portionwise at rt. The reaction was left under stirring for 48 h. After this period of time, the solvent was evaporated at reduced pressure, the residue was taken up with DCM, and the organic phase was washed with brine and finally dried over anhydrous Na_2SO_4. Upon evaporation of the solvent, the crude solid product **14** was collected, properly recrystallized, and fully characterized.

Compound ***15***. 0.86 g (89%), mp 193−194 °C from acetone-iPr_2O.

IR: ν = 3235 (NH), 1591 (C═N), 1521 (NO_2) cm^{-1}.

^{1}H NMR (300 MHz, $CDCl_3$, 25 °C): δ = 1.91 and 2.11 (d, 2H, J = 12 Hz, CH_2), 4.13 (d, 1H, J = 8 Hz, $H4_{Isox.}$), 4.14 (s, 1H, CH-N), 4.77 (s, 1H, CH−O), 4.79 (b, 1H, NH), 4.99 (d, 1H, J = 8 Hz, $H5_{Isox.}$), 7.65 (t, 1H, J = 8 Hz, arom.), 8.13 (d, 1H, J = 8 Hz, arom.), 8.30 (dd, 1H, J = 8, 1 Hz, arom.), 8.56 (d, 1H, J = 1 Hz, arom.).

^{13}C NMR (75 MHz, $CDCl_3$, 25 °C): δ = 34.7, 55.3, 59.0, 77.6, 84.4, 121.4, 124.8, 130.0, 130.1, 132.2, 148.5, 154.2.

$C_{12}H_{11}N_3O_4$ (261.24): HRMS: calcd (MW+H) 262.0822; found 262.0829.

Synthesis of Aminol 179. Compound **15** (0.76 g, 2.9 mmol) was dissolved in EtOAc (65 mL) along with 0.3 g C/Pd 10%, and the mixture was submitted to hydrogenation at rt. The reaction was left under stirring with a hydrogen stream until it absorbed 70 mL. After this, the solution was filtered, and the solvent was evaporated to dryness. The crude solid products **179** was recrystallized and fully characterized.

Compound ***179***. 0.76 g (99%), mp 180−182 °C from acetone-iPr_2O.

IR: ν = 3358 and 3291 (NH_2), 3086 (OH), 1588 (C═N), 1528 (NO_2) cm^{-1}.

^{1}H NMR (300 MHz, $CDCl_3$, 25 °C): δ = 1.79 and 1.88 (m, 2H, CH_2), 3.99 (d, 1H, J = 8 Hz, $H4_{Isox.}$), 4.24 (d, 1H, J = 4 Hz, CH-N), 4.46 (s, 1H, CH−O), 5.15 (b, 1H, OH), 5.38 (d, 1H, J = 8 Hz, $H5_{Isox.}$), 7.63 (t, 1H, J = 8 Hz, arom.), 8.16 (d, 1H, J = 8 Hz, arom.), 8.29 (d, 1H, J = 8 Hz, arom.), 8.34 (s, 1H, arom.).

^{13}C NMR (75 MHz, $CDCl_3$, 25 °C): δ = 38.6, 59.1, 65.0, 78.4, 93.7, 121.2, 124.5, 130.0, 130.9, 132.3, 154.7, 166.6.

$C_{12}H_{13}N_3O_4$ (263.25): HRMS: calcd (MW+H) 264.0979; found 264.0987.

Protection of Aminol 179. In a 250 mL flask, 1.0 g (3.8 mmol) of aminol **179** was dissolved in 100 mL of anhydrous DCM along with 0.57 mg (8.4 mmol) of imidazole. TBDMSCl (0.63 g, 4.2 mmol) was then added under stirring at room temperature, and the solution was left to react for 48 h. After this period of time, the solution was diluted with DCM and washed with brine (3 × 20 mL). The organic phase was dried over anhydrous Na_2SO_4. Upon evaporation of the solvent, a pale yellow oil relative to the protected compound **16** was obtained and fully characterized.

Compound ***16***. 0.82 g (57%), mp 95−96 °C from iPr_2O.

IR: ν = 3384 (NH_2), 1592 (C═N), 1528 (NO_2) cm^{-1}.

^{1}H NMR (300 MHz, $CDCl_3$, 25 °C): δ = 0.11 (s, 3H, CH_3), 0.13 (s, 3H, CH_3), 0.90 (s, 9H, CH_3), 1.60 and 1.88 (m, 2H, CH_2), 3.21 (m, 1H, CH-N), 3.33 (s, 2H, NH_2), 4.07 (dd, 1H, J = 10, 4 Hz, $H4_{Isox.}$), 4.26 (m, 1H, CH−O), 5.02 (dd, 1H, J = 10, 2 Hz, $H5_{Isox.}$), 7.77 (t, 1H, J = 8 Hz, arom.), 8.29 (dd, 2H, J = 8, 2 Hz, arom.), 8.69 (t, 1H, J = 2 Hz, arom.).

^{13}C NMR (75 MHz, $CDCl_3$, 25 °C): δ = −4.9, 17.7, 25.7, 42.2, 56.8, 60.5, 78.4, 93.2, 121.5, 124.4, 130.5, 133.2, 148.1, 157.1, 168.0.

$C_{18}H_{27}N_3O_4Si$ (377.52): HRMS: calcd (MW+H) 378.1844; found 378.1832.

Synthesis of Compound 17. In a 250 mL flask, 0.20 g (0.5 mmol) of amine **16** was dissolved in 120 mL of anhydrous DCM along with 0.23 g (0.6 mmol) of HBTU and 0.4 mL of DIPEA. Fmoc-Gly-OH (0.16 g, 0.5 mmol) was then added under stirring at room temperature, and the solution was left to react for 48 h. After this period of time, the organic phase is washed with brine and dried over anhydrous Na_2SO_4. Upon evaporation of the solvent, oily residues were collected, and product **17** was isolated from column chromatography and fully characterized.

Compound ***17***. 0.31 g (89%), mp 82−83 °C from iPr_2O.

https://doi.org/10.1021/acsomega.4c05480
ACS Omega 2024, 9, 41599−41615

IR: ν = 3392, 3310 (NH_2), 1722 (C═O), 1674 (C═O), 1592 (C═N), 1528 (NO_2) cm^{-1}.

^1H NMR (300 MHz, $CDCl_3$, 25 °C): δ = 0.11 (s, 3H, CH_3), 0.13 (s, 3H, CH_3), 0.90 (s, 9H, tBu), 1.72 and 1.95 (m, 2H, CH_2), 3.62 (m, 2H, CHN and CH-Fmoc.), 4.28 (m, 6H, CH_2O, $COCH_2N$, CHO, $H4_{Isox.}$), 5.03 (d, 1H, J = 10 Hz, $H5_{Isox.}$), 7.38 (m, 4H, arom.), 7.59 (m, 1H, NH), 7.74 (m, 3H, arom.), 7.82 (d, 2H, J = 8 Hz, arom. NH), 7.90 (d, 1H, J = 7 Hz, arom.), 8.22 (d, 2H, J = 8 Hz, arom.), 8.28 (d, 2H, J = 8 Hz, arom.), 8.54 (s, 1H, arom.).

^{13}C NMR (75 MHz, $CDCl_3$, 25 °C): δ = −5.0, 22.8, 25.7, 46.6, 52.3, 57.1, 65.8, 67.3, 78.1, 92.8, 120.1, 121.3, 124.4, 125.2, 127.1, 127.6, 130.0, 130.5, 133.3, 140.7, 143.8, 148.0, 156.2, 156.6, 168.4.

$C_{35}H_{40}N_4O_7Si$ (656.81): HRMS: calcd (MW+H) 657.2739; found 657.2729.

Synthesis of Compound 183. To solution of the compound **17** (0.26 g, 0.4 mmol) in anhydrous THF (50 mL), a 1 M solution of n-$Bu_4N^+F^-$ (0.3 mL, 0.3 mmol) was added under stirring at room temperature. The mixtures are left under stirring for 1 h. Then, the solutions were concentrated, taken up with DCM (150 mL), washed with brine (3 × 20 mL), and finally dried over Na_2SO_4. The crude solid product **183** was recrystallized and fully characterized.

*Compound **183***. 0.12 g (93%), mp 159−160 °C from iPr_2O.

IR: ν = 3343 and 3295 (NH_2), 3086 (OH), 1636 (C═O), 1592 (C═N), 1528 (NO_2) cm^{-1}.

^1H NMR (300 MHz, DMSO-d_6, 25 °C): δ = 1.84 (s, 2H, CH_2), 3.77 (m, 2H, CH_2), 4.29 (m, 2H, $H4_{Isox.}$, CH-N), 4.44 (m, 1H, CH−O), 5.09 (d, 1H, J = 9 Hz, $H5_{Isox.}$), 5.77 (d, J = 3 Hz, 1H, OH), 7.77 (t, 1H, J = 8 Hz, arom.), 8.29 (d, 1H, J = 8 Hz, arom.), 8.47 (m, 1H, J = 8 HZ, NH), 8.53 (d, 1H, J = 9 Hz, arom.), 8.72 (t, 1H, J = 2 Hz, arom.).

^{13}C NMR (75 MHz, DMSO-d_6, 25 °C): δ = 29.9, 36.4, 53.3, 53.7, 66.3, 76.7, 124.4, 130.3, 130.4, 133.4, 148.2, 155.5, 169.1, 169.6.

$C_{14}H_{16}N_4O_5$ (320.31): HRMS: calcd (MW+H) 321.1193; found 321.1191.

Computational Modeling. *Methods.* Computational experiments were conducted inside Schrodinger's Maestro v13.1.141 release 2022−1. Clustering analyses were performed using a GROMACS 2021. *Clustering.* The downloaded trajectory from the molecular dynamic (MD) SARS-CoV-2 database (PDB: 6LU7; model file ID: 520; trajectory file ID: 521; 500 μs; software and version: GROMACS 2020.2; FF: AMBER 99) was visualized with VMD and analyzed with a GROMACS 2021. An index file was generated from the model file and clustering analysis was performed (on Cα or selected residues indicated in allosteric site selection) using the method *gromos* with a cutoff of 0.2 nm. The most representative structures of each cluster were used in the subsequent analysis.

Modeling. The most representative conformations of the protein, identified through the clustering analysis, were prepared using Maestro; hydrogen atoms were added, and the protonation states were generated using PROPKA at pH 7.

Binding Site Identification. On the most representative structure of the protein, obtained through clustering analysis, pockets were searched using SiteMap, a module of Schrodinger's Maestro.

Database. The library of around 600 compounds was designed, based on the chemical pathways developed by our research unit.[14,28,35−44]

Docking. Grids for docking were generated using Glide, with the default settings. Ligands were built with the 3D Builder tool of Maestro and then prepared with LigPrep using force field OPLS4, and Epik was used to generate possible states at target pH 7 ± 2. Ligands were docked with extra precision in the predefined grids using Glide. Ten poses per ligand were generated, and postdocking minimization was performed. Optimal poses were chosen based on docking score, ligand efficiency, and interactions with selected residues − Arg298 for protease pocket 1, Ser1, Arg4, Lys5, and Glu290 for protease pocket 2. Ligand interaction diagrams (LID) of docked compounds were generated in a 2D workspace.

MD Simulations. Systems were prepared using Desmond's System Builder with the OPLS4 force field. Protein−ligand complexes were put into an orthorhombic box, surrounded by around 22,000 water molecules (SPC solvent model) with a buffer distance of 15 Å. The volume of the system was then minimized to around 1 × 10^6 Å. Negative charges in the system were neutralized by the addition of Na^+ ions. NaCl at a concentration of 0.15 M was also added.

Molecular dynamics trajectories were generated by using Schrodinger's Desmond. The NPT ensemble was used at a temperature of 300.0 K and pressure of 1.01325 bar. Prior to the simulation, the system was relaxed with the standard relaxation protocol of Desmond with default settings resulting in around 200 ps of equilibration. A Nosé−Hoover thermostat with a relaxation time of 1 ps and a Martyna−Tobias−Klein barostat with a relaxation time of 2 ps were used. The temperature and pressure couplings were set to isotropic. Simulations were run for 50 ns, and the trajectory was recorded each 20 ps.

Trajectory Analysis. Interactions with the protein and root-mean-square deviation (RMSD) were obtained through the simulation interactions diagram plugin of Maestro. Distances were calculated using Visual Molecular Dynamics (VMD); the protein was first centered in the box, and then frames were aligned. For the apo protein (i.e., protein without the prosthetic group), measurements were done one every 10 frames. Distances (Å) were measured throughout the course of the trajectory from the CZ and CD of the residue pair Arg4-Glu290, CZ and O (backbone) for the Arg298-Ser123 pair and the S atom of Cys145 to the hydrogen-donor nitrogen atom of His41 of the dimer complex (see Supporting Information, SI, Table S3 of amino acids nomenclature). Superposition of docking poses and frames of the trajectory was achieved by aligning the binding sites, considering residues within 8 Å from the pocket, through the align binding sites plugin of Maestro. Pairwise mean-square distance variations were calculated as described in ref 31; matrices were plotted with Gnuplot.[21]

Biological Assays. Human hepatocellular carcinoma cell line HepG2 (ATCC CCL-23) and human hepatocellular carcinoma cell line HepG2 (ATCC HB-8065), originally obtained from American Type Culture Collection (ATCC, Manassas, VA, USA) were maintained in 10% fetal bovine serum (FBS), 100 units/mL penicillin, 100 mg/mL streptomycin, and 2 mM L-glutamine supplemented RPMI 1640 (all from Euroclone, Milan, Italy) at 37 °C/5% CO_2.

The compounds **11**, **62**, **177**, **179**, **181**, **189**, and **193** were tested against the mutated NSP5 protease of the Omicron variant (P132H), with concentrations ranging from 0.1 to 100 μM. The control inhibitor (GC-376) was employed at a concentration of 50 μM. The assay (BPS Bioscence, San Diego, CA, USA) is designed to measure the NSP5 protease

https://doi.org/10.1021/acsomega.4c05480
ACS Omega 2024, 9, 41599−41615

activity by monitoring the cleavage of a fluorogenic-specific substrate. The NSP5 protease substrate is an internally quenched 14-mer fluorogenic (FRET) peptide (DABCYLKTSAVLQSGFRKME-EDANS). When the donor (EDANS) and acceptor (DABCYL) fluorophores are in close proximity, the energy emitted from EDANS is quenched by DABCYL (intact substrate). Upon proteolysis by NSP5 protease, the peptide substrate is cleaved to generate the highly fluorescent peptide fragment (SGFRKME-EDANS). The fluorescence intensity, which increases with protease activity, was quantified using a Fluoroskan microtiter plate-reading fluorimeter (Thermo Fisher Scientific, Waltham, MA, USA) with excitation at 360 nm and emission at 460 nm.

■ ASSOCIATED CONTENT

Supporting Information

The Supporting Information is available free of charge at https://pubs.acs.org/doi/10.1021/acsomega.4c05480.

^{1}H and ^{13}C NMR spectra and HRMS spectra of newly synthesized compounds. Docking Scores and Ligand efficiencies. Protein−ligand interaction diagrams. Distance fluctuation matrices (PDF)

■ AUTHOR INFORMATION

Corresponding Authors

Francesca Marino-Merlo − *Department of Chemical, Biological, Pharmaceutical, and Environmental Sciences, University of Messina, Messina 98166, Italy*; Email: francesca.marino@unime.it

Giulia Morra − *Biocomputing Lab, SCITEC-Istituto di Scienze e Tecnologie Chimiche CNR, Milano 20131, Italy*; orcid.org/0000-0002-9681-7845; Email: giulia.morra@scitec.cnr.it

Paolo Quadrelli − *Department of Chemistry, INSTM Research Unit of Pavia; University of Pavia, Pavia 27100, Italy*; orcid.org/0000-0001-5369-9140; Email: paolo.quadrelli@unipv.it

Authors

Marco Leusciatti − *Department of Chemistry, INSTM Research Unit of Pavia; University of Pavia, Pavia 27100, Italy; Biocomputing Lab, SCITEC-Istituto di Scienze e Tecnologie Chimiche CNR, Milano 20131, Italy*

Beatrice Macchi − *Department of Chemical Science and Technology, University of Rome Tor Vergata, Roma 00133, Italy*

Valeria Stefanizzi − *Department of Chemical, Biological, Pharmaceutical, and Environmental Sciences, University of Messina, Messina 98166, Italy*

Antonio Mastino − *Department of Chemical, Biological, Pharmaceutical, and Environmental Sciences, University of Messina, Messina 98166, Italy; The Institute of Translational Pharmacology, CNR, Roma 00133, Italy*

Complete contact information is available at: https://pubs.acs.org/10.1021/acsomega.4c05480

Author Contributions

All authors have given approval to the final version of the manuscript.

Notes

The authors declare no competing financial interest.

In this POC, the syntheses of compounds **11**, **62**, **177**, **179**, **181**, **189**, and **193** were conducted according to the well-established methodology as reported in references 13−29, leading to the desired products in the racemic forms. The regioisomers **4a,b**, **7a,b**, and **14a,b** were hence fast obtained in a very simple and reliable way. This protocol, in fact, allows for the preparation of consistent amounts of nucleosides at a high level of purity. The optimization of the other synthetic steps required the availability of good amounts of the starting materials to finalize the very last step of the planned syntheses. The enantiomeric resolution has been planned by using chiral acids or amines in a second phase of the study, after collecting the biological data, structural evaluation, and suitable outlined synthetic changes.

■ ACKNOWLEDGMENTS

Financial support by INSTM (Firenze) and the University of Pavia are gratefully acknowledged. This work was also supported by PRIN 2022 grant number W97H54_003 "Founded by European Union - Next Generation EU". We also thank Steroid S.p.A. and Curia S.r.l. for their financial support to research activities.

■ REFERENCES

(1) Kandwal, S.; Fayne, D. Genetic conservation across SARS-CoV-2 non-structural proteins − Insights into possible targets for treatment of future viral outbreaks. *Virology* **2023**, *581*, 97−115.

(2) Maxmen, A. More than 80 clinical trials launch to test coronavirus treatments. *Nature* **2020**, *578*, 347−348.

(3) Leusciatti, M.; Macchi, B.; Marino-Merlo, F.; Mastino, A.; Morra, G.; Quadrelli, P. Inhibition of the RNA-dependent RNA-polymerase from SARS-CoV-2 by 6-chloropurine isoxazoline-carbocyclic monophosphate nucleotides. *ACS Omega* **2023**, *8*, 36311−36320.

(4) Gao, Y.; Yan, L.; Huang, Y.; Liu, F.; Zhao, Y.; Cao, L.; Wang, T.; Sun, Q.; Ming, Z.; Zhang, L.; Ge, J.; Zheng, L.; Zhang, Y.; Wang, H.; Zhu, Y.; Zhu, C.; Hu, T.; Hua, T.; Zhang, B.; Yang, X.; Li, J.; Yang, H.; Liu, Z.; Xu, W.; Guddat, L. W.; Wang, Q.; Lou, Z.; Rao, Z. Structure of the RNA-dependent RNA polymerase from COVID-19 virus. *Science* **2020**, *368*, 779−782.

(5) Goodsell, D. S.*RCSB PDB-101*. 2020, doi:.

(6) Goyal, B.; Goyal, D. Targeting the Dimerization of the Main Protease of Coronaviruses: A Potential Broad-Spectrum Therapeutic Strategy. *ACS Comb. Sci.* **2020**, *22*, 297−305.

(7) Hu, Q.; Xiong, Y.; Zhu, G. H.; Zhang, Y. N.; Zhang, Y. W.; Huang, P.; Ge, G. B. The SARS-CoV-2 main protease (M^{pro}): Structure, function, and emerging therapies for COVID-19. *MedComm* **2022**, *3*, No. e151.

(8) Cannalire, R.; Cerchia, C.; Beccari, A. R.; Di Leva, F. S.; Summa, V. Targeting SARS-CoV-2 Proteases and Polymerase for COVID-19 Treatment: State of the Art and Future Opportunities. *J. Med. Chem.* **2022**, *65*, 2716−2746.

(9) Günther, S.; et al. *(92 authors)* X-ray screening identifies active site and allosteric inhibitors of SARS-CoV-2 main protease. *Science* **2021**, *372*, 642−646.

(10) Alzyoud, L.; Mahgoub, R. E.; Mohamed, F. E.; Ali, B. R.; Ferreira, J.; Rabeh, W. M.; Atatreh, N.; Ghattas, M. A. The Discovery of Novel Small Oxindole-Based Inhibitors Targeting the SARS-CoV-2 Main Protease (M^{pro}). *Chem. Biodiversity* **2023**, *20*, No. e202301176.

(11) Arutyunova, E.; Khan, M. B.; Fischer, C.; Lu, J.; Lamer, T.; Vuong, W.; van Belkum, M. J.; McKay, R. T.; Tyrrell, D. L.; Vederas, J. C.; Young, H. S.; Lemieux, M. J. N-Terminal Finger Stabilizes the S1 Pocket for the Reversible Feline Drug GC376 in the SARS-CoV-2 M^{pro} Dimer. *J. Mol. Biol.* **2021**, *433*, No. 167003.

(12) Lamb, Y. N. Nirmatrelvir Plus Ritonavir: First Approval. *Drugs* **2022**, *82*, 585−591.

(13) Zhang, L.; Lin, D.; Sun, X.; Curth, U.; Drosten, C.; Sauerhering, L.; Becker, S.; Rox, K.; Hilgenfeld, R. Crystal structure of SARS-CoV-2 main protease provides a basis for design of improved α-ketoamide inhibitors. *Science* **2020**, *368*, 409−412.
(14) Alzyoud, L.; Ghattas, M. A.; Atatreh, N. Allosteric Binding Sites of the SARS-CoV-2 Main Protease: Potential Targets for Broad-Spectrum Anti-Coronavirus. *Agents. Drug Des. Devel. Ther.* **2022**, *16*, 2463−2478.
(15) Quadrelli, P. Eds. "*Modern Applications of Cycloaddition Chemistry*", Elsevier: Amsterdam, 2019; pp 1−152.
(16) Memeo, M. G.; Quadrelli, P. Generation and trapping of nitrosocarbonyl intermediates. *Chem. Rev.* **2017**, *117*, 2108−2200.
(17) Moggio, Y.; Legnani, L.; Bovio, B.; Memeo, M. G.; Quadrelli, P. Synthesis of novel anthracene derivatives of isoxazolino-carbocyclic nucleoside analogues. *Tetrahedron* **2012**, *68*, 1384−1392.
(18) Quadrelli, P.; Scrocchi, R.; Caramella, P.; Rescifina, A.; Piperno, A. From cyclopentadiene to isoxazoline−carbocyclic nucleosides: a rapid access to biological molecules through nitrosocarbonyl chemistry. *Tetrahedron* **2004**, *60*, 3643−3651.
(19) Quadrelli, P.; Mella, M.; Carosso, S.; Bovio, B. *N,O*-Nucleosides from Ene Reactions of Nitrosocarbonyl Intermediates with the 3-Methyl-2-buten-1-ol. *J. Org. Chem.* **2013**, *78*, 516−526.
(20) Aljaf, K. K.; Amin, A. A.; Hussain, F. H. S.; Quadrelli, P. DEAE-cellulose-catalyzed synthesis of 5-hydroxy-isoxazolidines and their synthetic uses towards nucleoside analogues. *Arkivoc* **2020**, *2020*, 73−83.
(21) Morra, G.; Neves, M. A. C.; Plescia, C. J.; Tsustsumi, S.; Neckers, L.; Verkhivker, G.; Altieri, D. C.; Colombo, G. Dynamics-Based Discovery of Allosteric Inhibitors: Selection of New Ligands for the C-terminal Domain of Hsp90. *J. Chem. Theory Comput.* **2010**, *6*, 2978−2989.
(22) Torrens-Fontanals, M.; Peralta-García, A.; Talarico, C.; Guixà-González, R.; Giorgino, T.; Selent, J. SCoV2-MD: a database for the dynamics of the SARS-CoV-2 proteome and variant impact predictions. *Nucleic Acids Res.* **2022**, *50*, D858−D866.
(23) del Sol, A.; Tsai, C.-J.; Ma, B.; Nussinov, R. The Origin of Allosteric Functional Modulation: Multiple Pre-existing Pathway. *Structure* **2009**, *17*, 1042−1050.
(24) Hu, T.; Zhang, Y.; Li, L.; Wang, K.; Chen, S.; Chen, J.; Ding, J.; Jiang, H. Two adjacent mutations on the dimer interface of SARS coronavirus 3C-like protease cause different conformational changes in crystal structure. *Virology* **2009**, *388*, 324−334.
(25) El-Baba, T. J.; Lutomski, C. A.; Kantsadi, A. L.; Malla, T. R.; John, T.; Mikhailov, V.; Bolla, J. R.; Schofield, C. J.; Zitzmann, N.; Vakonakis, I.; Robinson, C. V. Allosteric Inhibition of the SARS-CoV-2 Main Protease: Insights from Mass Spectrometry Based Assays. *Angew. Chem., Int. Ed.* **2020**, *59*, 23544−23548.
(26) Quadrelli, P.; Scrocchi, R.; Caramella, P.; Rescifina, A.; Piperno, A. From cyclopentadiene to isoxazoline−carbocyclic nucleosides: a rapid access to biological molecules through nitrosocarbonyl chemistry. *Tetrahedron* **2004**, *60*, 3643−3651.
(27) Quadrelli, P.; Mella, M.; Carosso, S.; Bovio, B. *From the* Ene Reaction of Nitrosocarbonyl Intermediates with the 3-Methyl-but-2-en-1-ol, a New Class of Purine *N. O-Nucleoside Analogues. Synthesis* **2013**, *45*, 1414−1420.
(28) Quadrelli, P.; Mella, M.; Legnani, L.; Al-Saad, D. From Cyclopentadiene to Isoxazoline-Carbociclic Nucleosides; Synthesis of Highly Active Inhibitors of Influenza A Virus H1N1. *Eur. J. Org. Chem.* **2013**, *2013*, 4655−4665.
(29) Memeo, M. G.; Mella, M.; Montagna, V.; Quaderelli, P. Design, Synthesis, and Conformational Analysis of Proposed β-Turn Mimics from Isoxazoline-Cyclopentane Aminols. *Chem.—Eur. J.* **2015**, *21*, 16374−16378.
(30) Aljaf, K. K.; Amin, A. A.; Hussain, F. H. S.; Quadrelli, P. Diethylaminoethyl cellulose (DEAE-C): applications in chromatography and in organic synthesis. *Arkivoc* **2020**, *2020*, 153−179.
(31) Ma, C.; Sacco, M. D.; Townsend, J. A.; Hu, Y.; Szeto, T.; Zhang, X.; Tarbet, B.; Marty, M. T.; Chen, Y.; Wang, J. Boceprevir, GC-376, and calpain inhibitors II, XII inhibit SARS-CoV-2 viral replication by targeting the viral main protease. *Cell Res.* **2020**, *30*, 678−692.
(32) Caramella, P.; Grünanger, P. *1,3-Dipolar Cycloaddition Chemistry.*; Padwa, A., Eds.; John Wiley & Sons Inc.: New York, 1984, Vol. *1*, p 291−392.
(33) Grünanger, P.; Finzi, P. V. *Isoxazoles*; John Wiley & Sons, Inc.: New York, 1999, Vol. *1 and 2*.
(34) Grundmann, C.; Grünanger, P. *The Nitrile Oxides*; Springer-Verlag: Heidelberg, 1971.
(35) Presenti, P.; Moiola, M.; Quadrelli, P. 5-Hydroxy-isoxazolidine: A New Synthetic Approach to a Privileged Heterocycle for Organic Synthesis. *Chemistry Select* **2020**, *5*, 5367−5373.
(36) Scagnelli, L.; Memeo, M. G.; Carosso, S.; Bovio, B.; Quadrelli, P. Syntheses of New Carbanucleosides by Pericyclic Reactions. *Eur. J. Org. Chem.* **2013**, 3835−3846.
(37) Al-Saad, D.; Memeo, M. G.; Quadrelli, P. Pericyclic Reactions for Anti-HPV Antivirals: Unconventional Nucleoside Analogue Synthesis via Nitrosocarbonyl Chemistry. *Chemistry Select* **2017**, *2*, 10340−10346.
(38) Carella, S.; Memeo, M. G.; Quadrelli, P. Electrocyclic Ring-Opening of 1,2,4-Oxadiazole[4,5-*a*]pyridinium Chloride: a New Route to 1,2,4-Oxadiazole Dienamino Compounds. *Chemistry Open* **2019**, *8*, 1209−1221.
(39) Mantione, D.; Aizpuru, O. O.; Memeo, M. G.; Bovio, B.; Quadrelli, P. 4-Heterosubstituted Cyclopentenone Antiviral Compounds: Synthesis, Mechanism, and Antiviral Evaluation. *Eur. J. Org. Chem.* **2016**, 983−911.
(40) Moggio, Y.; Legnani, L.; Bovio, B.; Memeo, M. G.; Quadrelli, P. Synthesis of novel anthracene derivatives pf isoxazolino-carbocyclic nucleoside analogues. *Tetrahedron* **2012**, *68*, 1384−1392.
(41) Savion, M.; Memeo, M. G.; Bovio, B.; Grazioso, G.; Legnani, L.; Quadrelli, P. Synthesis and molecular modeling of novel dihydroxycyclopentane-carbonitrile nor-nucleosides by bromonitrile oxide 1,3-dipolar cycloaddition. *Tetrahedron* **2012**, *68*, 1854−1852.
(42) Al-Saad, D.; Memeo, M. G.; Quadrelli, P. Pericyclic Reactions for Antivirals: Synthesis of 4-Bromo-*N*-[(1*R**,4*S**)-4-hydroxy-2-cyclohexen-1-yl]-2-thiazolecarboxamide. *Lett. Org. Chem.* **2017**, *13*, 757−763.
(43) Corti, M.; Leusciatti, M.; Moiola, M.; Mella, M.; Quadrelli, P. Nitrosocarbonyl Carbohydrate Derivatives: Hetero Diels-Alder and Ene Reaction Products for Useful Organic Synthesis. *Synthesis* **2021**, *53*, 574−586.
(44) Al-Saad, D.; Memeo, M. G.; Quadrelli, P. #Nitrosocarbonyls 1: Antiviral Activity of *N*-(4-Hydroxycyclohex-2-en-1-yl)quinoline-2-carboxamide against the Influenza A Virus H1N1. *Sci. World J.* **2014**, No. 472373.

https://doi.org/10.1021/acsomega.4c05480
ACS Omega 2024, 9, 41599−41615